



Review

# Trends and Applications of Surface and Bulk Acoustic Wave Devices: A Review

Yang Yang \* , Corinne Dejous and Hamida Hallil \*

University of Bordeaux, CNRS, Bordeaux INP, IMS UMR 5218, F33400 Talence, France

\* Correspondence: yang.yang@u-bordeaux.fr (Y.Y.); hamida.hallil-abbas@u-bordeaux.fr (H.H.)

**Abstract:** The past few decades have witnessed the ultra-fast development of wireless telecommunication systems, such as mobile communication, global positioning, and data transmission systems. In these applications, radio frequency (RF) acoustic devices, such as bulk acoustic waves (BAW) and surface acoustic waves (SAW) devices, play an important role. As the integration technology of BAW and SAW devices is becoming more mature day by day, their application in the physical and biochemical sensing and actuating fields has also gradually expanded. This has led to a profusion of associated literature, and this article particularly aims to help young professionals and students obtain a comprehensive overview of such acoustic technologies. In this perspective, we report and discuss the key basic principles of SAW and BAW devices and their typical geometries and electrical characterization methodology. Regarding BAW devices, we give particular attention to film bulk acoustic resonators (FBARs), due to their advantages in terms of high frequency operation and integrability. Examples illustrating their application as RF filters, physical sensors and actuators, and biochemical sensors are presented. We then discuss recent promising studies that pave the way for the exploitation of these elastic wave devices for new applications that fit into current challenges, especially in quantum acoustics (single-electron probe/control and coherent coupling between magnons and phonons) or in other fields.

**Keywords:** RF acoustic devices; SAW; BAW; sensor application; RF filter; physical transducers; biochemical transducers



**Citation:** Yang, Y.; Dejous, C.; Hallil, H. Trends and Applications of Surface and Bulk Acoustic Wave Devices: A Review. *Micromachines* **2023**, *14*, 43. <https://doi.org/10.3390/mi14010043>

Academic Editors: Hongping Hu, Pei-Hsun Wang and Zhenghua Qian

Received: 18 November 2022

Revised: 20 December 2022

Accepted: 21 December 2022

Published: 24 December 2022



**Copyright:** © 2022 by the authors. Licensee MDPI, Basel, Switzerland. This article is an open access article distributed under the terms and conditions of the Creative Commons Attribution (CC BY) license (<https://creativecommons.org/licenses/by/4.0/>).

## 1. Introduction

In recent decades, the rapid development of microwave wireless communication technology has led to very rapid developments in other fields, such as mobile communication systems (CDMA, UMTS, GSM, etc.), global positioning systems (GPS, Galileo, etc.), data transmission systems (such as WLAN, Bluetooth, etc.), satellite communication, and other military communication systems [1]. The most important parts of the components that make up these systems, such as filters, duplexers, voltage-controlled oscillators, frequency meters, and tunable amplifiers, are microwave resonators [2]. With the remarkable advances in microelectronics and microfabrication technologies, researchers have paid more attention to the miniaturization and integration of devices while improving their performance. They have succeeded in integrating multiple devices on a single chip and in accommodating active and passive devices or MEMS devices in a single package [3].

Conventional microwave resonators use electromagnetic waves as energy carriers. In the RF/microwave frequency range, the required resonators have dimensions that can hardly meet the integration requirements for applications such as the current fifth-generation (5G) telecommunication standard. With wave velocities four to five orders of magnitude slower than that of electromagnetic waves, acoustic waves allow a reduction of device dimensions in the same proportions [4]. As a consequence, acoustic wave devices can meet the current miniaturization and integration requirements [5].

This paper aims to present an overview of surface and bulk acoustic waves technologies and of major application fields in a comprehensive manner, especially for the

benefit of novice readers, because a profusion of literature is associated with such quickly expanding technologies. We first present the basic principles of SAW and BAW devices, typical structures, main characterizations, potential limitations, and possible optimization methods. Regarding BAW devices, we give particular attention to the film bulk acoustic resonator (FBAR), which holds a higher operation frequency and a better integration capacity compared with SAW devices. We then propose an overview of major current applications, which is divided into three parts: RF signal filters, physical sensors and actuators, and chemical and biochemical sensors. Finally, we conclude this review with a brief introduction to current trends associated with quantum acoustics and some applications.

## 2. Basic Principles of SAW and BAW Devices

Acoustic components are based on acoustic waves generated from the piezoelectric effect, one of the most exciting material properties. The term derives from the Greek word *piezein* (to press), and the effect is based on an interaction between an electrical charge and mechanical stress [6]. In 1880, the Curie brothers discovered that applying pressure or tension in a certain direction to a quartz crystal results in the formation of electrical charges on its surface, and the density of the electrical charge is proportional to the magnitude of the applied external force [7]. This is the positive piezoelectric effect of piezoelectric materials. One year later, the Curie brothers proved the inverse effect through experiments and determined the direct and inverse piezoelectric coefficients of quartz crystal [8].

Acoustic waves generated from the piezoelectric effect can be broadly classified into two types: BAW [9] and SAW [10]. Essentially, BAW are generated by an alternating (AC) electrical signal applied between the two sides of the piezoelectric material, and the acoustic wave propagates through the entire thickness, giving rise to a stationary wave at specific frequencies. Depending on the crystalline orientation, the piezoelectric material can expand and contract perpendicularly to the surface as in Figure 1a; the wave polarization is longitudinal, as the mechanical displacement is parallel to the propagation direction; such a mode is called thickness-extension mode. When the piezoelectric material deforms in a direction parallel to the surface, the mode is called thickness-shear mode, as in Figure 1b [11]. In the case of SAW, the vibrations occur only at the surface of the material. By placing interdigitated transducers (IDTs) on the surface of the piezoelectric material, as in Figure 1c, the propagating SAW will be generated when an AC signal is applied; the resonance frequency, amplitude, and propagation characteristics are determined by the design of the IDTs, the dimensions of the electrodes, the material properties, and the applied electrical signal. As for the BAW, several types of polarization and modes exist; some of the most significant ones are described in the following part.

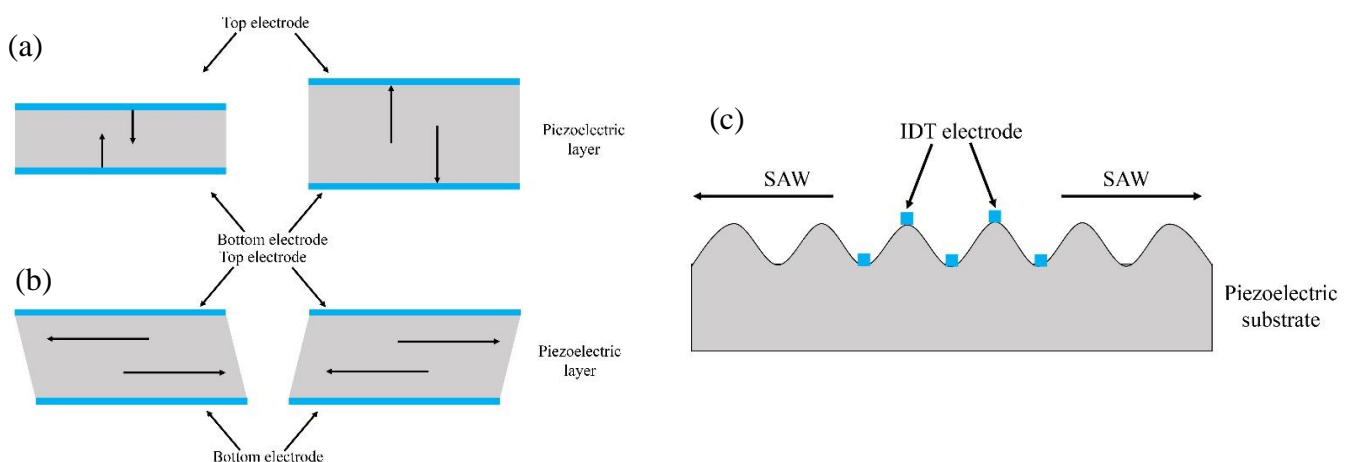


**Figure 1.** Profiles of (a) thickness-extensional mode and (b) thickness-shear mode of a BAW device; (c) SAW.

### 2.1. Basic Structures

In 1885, Lord Rayleigh discovered the “Waves Propagated along the Plane Surface of an Elastic Solid” and defined the first discovered SAW, which were named Rayleigh waves [12]. Rayleigh waves cause surface particles to move elliptically in planes perpendicular to the surface and parallel to the propagation direction. They are typically involved in seismic movements. In 1911, Augustus Edward Hough Love mathematically predicted the existence of so-called Love waves, which can propagate when the surface of a semi-infinitely thick elastic body is covered with a layer of a medium with lower sound velocity. The Love wave is a guided shear horizontal surface wave (SH-SAW) with a displacement of the particles parallel to the surface [13]. In 1965, Richard Manning White et al. proposed to directly deposit interdigital transducers (IDTs) onto the surface of piezoelectric materials in order to generate, transmit, and receive SAW efficiently [14]. As represented in Figure 2a, in a standard SAW resonator with a delay line, when the electrical signal arrives at the input IDT (left side) through a feedline, here with matching dipole, acoustic waves are generated by the inverse piezoelectric effect and acoustic resonance occurs, at specific frequencies of constructive waves, for which acoustic waves travel across the propagation path. Arriving at the output IDT (right side), the acoustic signal is therefore converted back into an electrical signal through the output feedline by the piezoelectric effect.

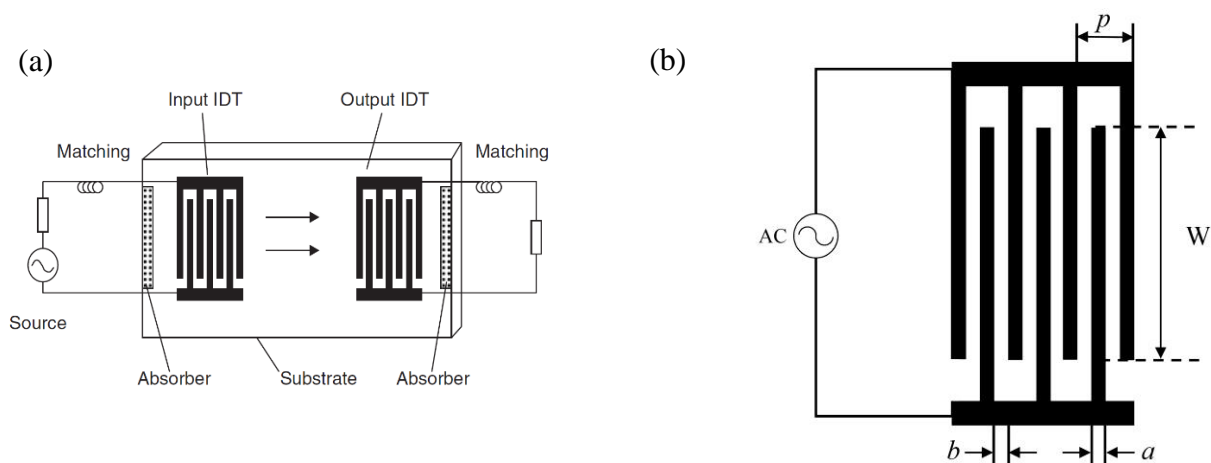


**Figure 2.** (a) Schematic diagram of classic SAW resonator with delay line, adapted with permission from [4]; (b) the classic structure of IDT.

Indeed, the IDT is a typical electroacoustic conversion structure in SAW filters and other SAW devices. Its basic design is shown in Figure 2b, with metal strips on the piezoelectric substrate intertwined and connected to the signal and the ground, alternately. These interdigitated electrodes are structurally characterized by the finger width  $a$ , interfinger distance  $b$ , acoustic aperture  $W$ , spatial periodicity  $p$ , and number of finger pairs  $N$ . When an IDT is connected to an alternating signal source, the material is deformed locally due to the converse piezoelectric effect. At the resonance frequency, the waves emitted by each pair of electrodes are constructive and the resulting SAW propagate in the two opposite directions perpendicular to the fingers. The acoustic signals reaching the second IDT are converted into electrical signals due to the piezoelectric effect. Although the two transducers are reciprocal, for simplicity, the transducer connected to the alternating signal source will be referred to as the exciting or input IDT and the transducer connected to the load will be referred to as the receiving or output IDT. The acoustic resonance frequency is expressed as

$$f_0 = \frac{v_s}{p} \quad (1)$$

and the angular frequency

$$\omega_0 = 2\pi \frac{v_s}{p} \quad (2)$$

where  $v_s$  is the velocity of the SAW, which depends on the piezoelectric substrate properties in the considered orientation, and the spatial periodicity  $p$  of the IDTs is equal to the wavelength  $\lambda$  of the propagating SAW.

Unlike SAW resonators, BAW resonators use acoustic waves which propagate in the direction of the thickness of the piezoelectric material. The thickness of the piezoelectric plate typically corresponds to half a wavelength ( $\lambda/2$ ) of the fundamental resonance frequency of the thickness-extensional mode (Figure 3), which can be expressed as follows, assuming infinitely thin electrodes:

$$f_r = \frac{v_L}{2h} \quad (3)$$

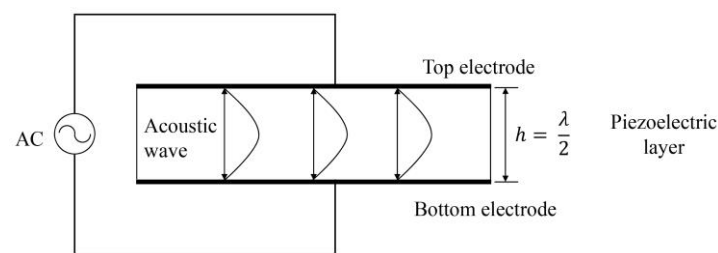


**Figure 3.** Schematic diagram of BAW resonator.

Here  $h$  is the thickness of the piezoelectric layer, and  $v_L$  is the velocity of longitudinal waves in the piezoelectric medium in the plate thickness direction.

Though such devices are widely used based on bulk piezoelectric materials, like clock sources and quartz crystal microbalances (QCMs), Equation (3) highlights the need for very thin plates for high frequency operation, not compatible with bulk materials. As a consequence, due to the limitations of the fabrication process, the performance of conventional BAW resonators remained lower compared with that of the SAW resonators. In parallel, piezoelectric layer-based devices have been investigated. In 1965, Newell first proposed a piezoelectric sandwich resonator structure using an acoustic Bragg reflector with thickness layers of  $\lambda/4$  and indicated that it was likely to be used in the high-frequency range [15]. In 1967, Sliker and Roberts proposed a CdS-based acoustic resonator on a quartz wafer [16], and the theoretical model of the device was basically mature at this time. In 1980, Grudkowski et al. proposed the concept of a BAW resonator filter and fabricated a ZnO-based BAW filter on a Si substrate with an operating frequency of 200~500 MHz [17]. In 1981, Lakin et al. clarified for the first time the application perspectives of thin-film bulk acoustic resonators (TFBARs) [18].

With the development of microfabrication processes, the advantages of BAW resonators slowly began to appear by the end of the 20th century. In 1996, Ruby prepared a BAW resonator based on a piezoelectric AlN film with a quality factor (Q value) of 2300 and an electromechanical coupling coefficient  $k_t^2$  of 6% [19]. Q value is a dimensionless ratio of the stored energy to the energy loss within a resonant element. He then investigated and prepared a 1900 MHz duplexer based on a film bulk acoustic waves resonator (FBAR) [20]. At this time, FBARs gradually began to be commercialized, which prompted more companies to conduct research on FBARs. In 2001, Agilent (i.e., Avago Avago) first introduced the PCS (personal communications systems) duplexer with an operation frequency of 1900 MHz for the mobile phone market [20], which was already in mass production at that time, officially initiating the commercial move of FBARs. The German company Infineon [21] then also launched its own BAW devices. Later, Intel [22], TriQuint [23] in the United States, Philips [24] in the Netherlands, and Samsung [25] in South Korea joined the development of BAW resonators.

Conventional QCM type BAW devices have been well-investigated, with a variety of fundamental and harmonic modes. We focus on the emerging thin-film-type FBAR, with some outstanding features compared with the classical BAW and even SAW. The current FBAR devices can be divided into two main types by their structures: the front-side etch or airbag type and the solidly mounted type (solidly mounted resonators; SMRs). Both are based on the same principles; the main difference is the method of energy confinement. In the FBAR, an air cavity with a length and width of 100–300  $\mu\text{m}$  is etched under the bottom electrode in order to obtain a suspended piezoelectric membrane confining the acoustic energy, as illustrated in Figure 4a [26]. In the SMR structure, a “mirror” under the electrode reflects acoustic waves. As shown in Figure 4b, these acoustic Bragg reflectors alternate layers of different acoustic impedances, such as W and  $\text{SiO}_2$  (impedance ratio of about 4:1), AlN and  $\text{SiO}_2$  (impedance ratio of about 3:1). By reflecting acoustic waves back to the piezoelectric film, they play a role in limiting energy dissipation [27]. To design the acoustic Bragg reflectors, the acoustic impedance of each material layer can be calculated as follows:

$$Z_a = \rho v_L \quad (4)$$

where  $\rho$  is the material density and  $v_L$  is the velocity of the longitudinal wave in the film thickness direction if considering the SMR thickness-extensional mode.

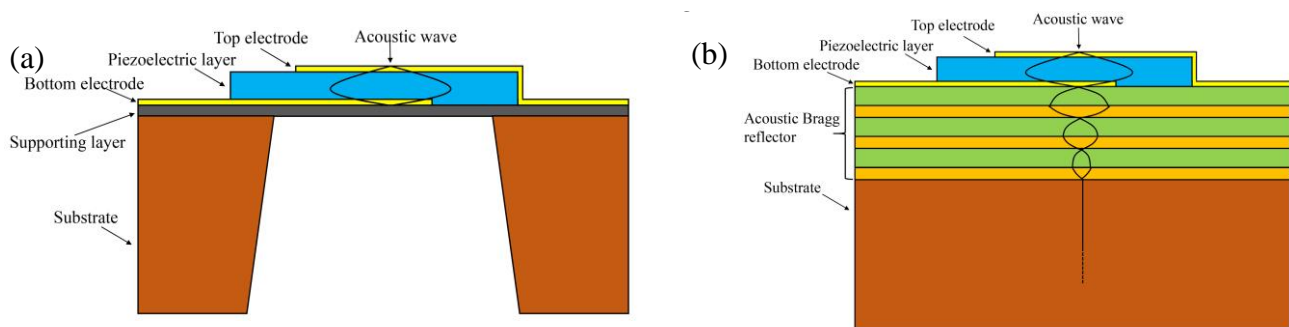


**Figure 4.** (a) Conventional FBAR structure; (b) SMR-type FBAR structure.

The differences in structure and acoustic reflection of the two resonators determine the differences in their fabrication, performance, and applications. In terms of design and fabrication, the longitudinal acoustic waves are confined in the FBAR membrane, the design is flexible, and the processing is quite simple due to the smaller number of layers [28]. In the design of SMR, not only does the lateral acoustic energy dissipation need to be considered (the impact brought by the lateral acoustic modes is presented below), but the design of the acoustic Bragg reflector is also critical as it directly impacts the energy dissipation and the performance of the resonator. To ensure the Q value, a fine control of the thickness during processing is also required [26].

As for performance, FBAR has a higher effective electromechanical coupling coefficient ( $k_{eff}^2$ ) [28], with a larger difference in acoustic impedance at the electrode–air interface than at the junction with the Bragg reflector of the SMR structure. Furthermore, the Bragg reflector adds some new loss mechanisms that reduce its Q value. However, the SMR structure also offers some interests. Indeed, the multiple  $\text{SiO}_2$  layers of the Bragg reflector have a negative temperature coefficient of frequency (TCF), which provides a matching effect on the TCF of the whole SMR [26]. Second, the FBAR membrane is mechanically supported at the edge of the cavity structure, which is risky during the microfabrication process, and the stress of the film must be carefully controlled to avoid mechanical cracking. On the contrary, the SMR structure does not suffer from such drawbacks, provided there are stable layer interfaces [9].

### 2.2. Typical Characterizations

SAW devices are usually electrically characterized by their scattering parameters (S-parameters),  $S_{ij}$  corresponding to the output power at port  $i$  divided by the input power at port  $j$ , or transmission gain from port  $j$  to port  $i$ .

Figure 5 gives an example of the characterization results of a SAW delay line (two-port device) such as those used by Rubé, M et al. [29], measured with a vector network analyzer (VNA) in the frequency domain. It exhibits a resonance at about 118 MHz, with a sharp dip in the reflection parameter  $S_{11}$ , which corresponds to a maximum of  $S_{21}$ , the transmission being supported by an acoustic wave between ports.

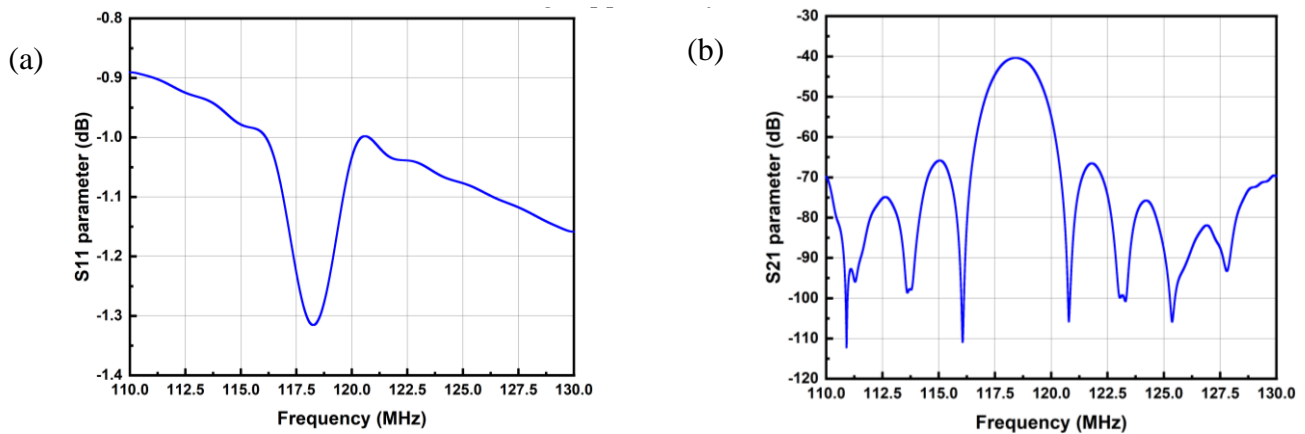


Figure 5. (a)  $S_{11}$  parameter; (b)  $S_{21}$  parameter of typical SAW resonator frequency response.

Among other applications, signal filtering is one of the most typical applications for SAW devices, for which they are designed to meet frame specifications, in terms of passband and stopband, as well as maximum and minimum losses inside, respectively.

In the above, we have presented the classic design of SAW devices. However, reflections on metal electrodes or other interfaces, material losses, and other spurious modes can highly influence the performances. Such effects can be reduced by an appropriate design, as described here.

The first important effect is the internal reflection at the metal strips of an IDT. This is illustrated in Figure 6a, with an electrode pitch equal to half the center frequency wavelength ( $\lambda_0/2$ ) resulting in an in-phase addition of the unwanted reflections at this frequency, which causes a significant impact on performances by causing ripples in the amplitude and phase. With a split-finger IDT, as shown in Figure 6b, the electrode pitch becomes  $\lambda_0/4$ , so that the reflections between two adjacent electrodes cancel each other, being  $180^\circ$  out of phase, and the overall reflected wave is cancelled.

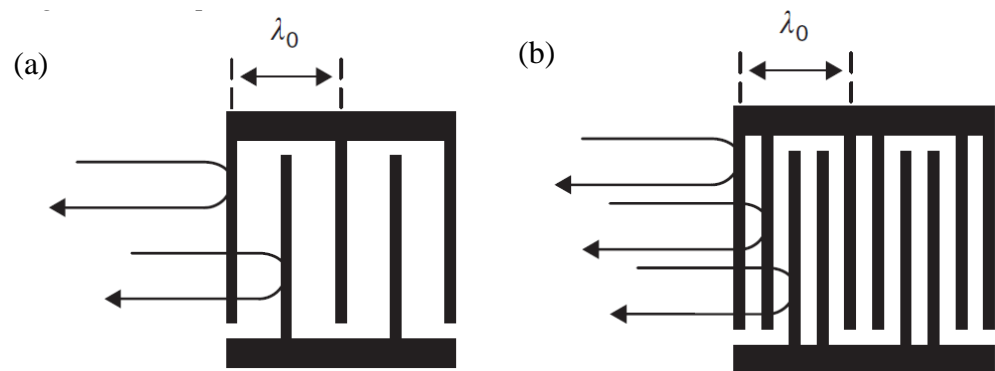
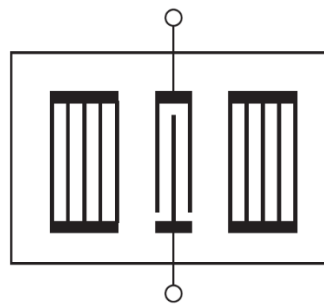


Figure 6. The reflection of SAW (a) single-electrode IDT; (b) split-finger electrode IDT, adapted with permission from [4].

In some designs, gratings on the surface are used to improve the confinement of acoustic energy in the transducer and consequently the Q value of the SAW device. In Figure 7, a one-port resonator has two such metallic side gratings, which act as two reflectors for the acoustic energy generated by the central IDT, therefore improving the Q value. Metallic gratings can not only provide mechanical but also electrical reflection, since an electrical field can also be formed by reflected acoustic waves due to the piezoelectric effect. The electrical characteristics of these reflections depend on the metal strips' electrical connections, either short-circuited as in Figure 7, or open-circuited, or a combination of them which is named as positive and negative reflection (PNR) grating, with enhanced reflection properties. Gratings are also widely used in two-port SAW delay-line structures [30]. Another way of limiting bidirectional losses lies on specific designs enabling control of internal reflections within the generating IDT itself, such as in a single-phase unidirectional transducer (SPUDT) [4].



**Figure 7.** One-port SAW resonator with gratings, adapted with permission from [4].

Spurious BAW modes are also a possible source of reduced performance. Among them, so-called deep bulk acoustic waves (DBAW) can be generated by the input IDT, then propagate in the volume of the piezoelectric layer, get reflected at the bottom face, and propagate back to the receiving IDT. Surface skimming bulk waves (SSBW) and other leaky waves are also examples of possibly interfering (or sometimes alternating) waves [31].

Waves undergoing reflections on the device sides or bottom can be limited by sandblasting the bottom surface or biasing the sides in order to avoid constructive reflections travelling back to the IDTs. Other interfering waves such as SSBW need, for intrinsic good design, to take into account both longitudinal and shear acoustic waves.

Other particular IDT structures can also be implemented during the design process in order to achieve a specific response pattern, such as apodization [32], weighted IDT transducers [33], multistrip couplers (MSCs) [34], etc.

All these optimizations aim to reduce the impacts of spurious modes or secondary effects, to better confine the acoustic energy and improve the Q value, and therefore to improve the performances of SAW devices.

The BAW devices have a single port; they are usually characterized by measuring their reflection coefficient  $S_{11}$ . As shown in Figure 8a, a minimum return loss is obtained near the resonance loss with a high Q value. For a BAW device with good performance, the Q value can reach several thousand [19,35,36].

In addition to  $S_{11}$ , the electrical impedance resulting from the theory of transmission lines [37] is an important characterization property for BAW devices, which can be expressed as

$$Z = \frac{1 + S_{11}}{1 - S_{11}} Z_0 \quad (5)$$

where  $Z$  is the electrical impedance of the device and  $Z_0$  is transmission line characteristic impedance, typically  $50 \Omega$  for a vector network analyzer (VNA).

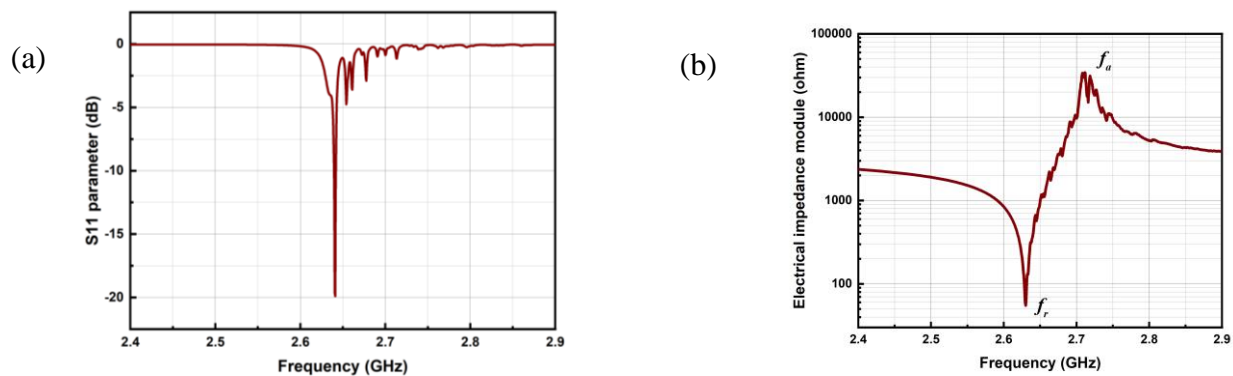


**Figure 8.** (a)  $S_{11}$  parameter and (b) electrical impedance of a 2.63 GHz ZnO based SMR (simulation results).

As is shown in Figure 8b, the electrical impedance  $Z$  reaches a minimum (tends to zero) at the resonance frequency  $f_r$ , which corresponds to a maximum of the mechanical deformation caused by the piezoelectric effect; at the antiresonance frequency  $f_a$ , the electrical impedance  $Z$  reaches a maximum (tends to infinity).

However, longitudinal deformations are accompanied by transverse ones, so that some lateral acoustic modes also propagate in BAW devices [38]. These unwanted acoustic modes, or spurious modes, are visible in the electrical response of the resonator in the form of parasitic resonances, in addition to the main one. These lateral acoustic waves travel between the boundaries of the active region of the piezoelectric layer, bounce off the electrode edges, and form lateral standing waves. Since they have to share the total energy, they are responsible for the degradation of the effective electromechanical coupling coefficient and of the Q value [26].

There are mainly two kinds of methods to improve this degradation caused by undesirable lateral modes. One method is called apodization. By using an asymmetrically shaped top electrode [39], most of the standing lateral waves are smeared out between the electrode edges and fewer parasitic resonances are observed in the electrical response. The most commonly used shapes of BAW top electrodes are irregular squares, pentagons, and circles. Another method is to build a frame around the edge of the top electrode [40]. By carefully designing the width and thickness of the frame, the different orders of lateral modes couple together and are vanished. This is an efficient method for suppressing unwanted modes, confining energy, and obtaining a smooth electrical response and a better Q factor [40]. However, due to the complexity of this structure and the difficulties in processing, the apodization method is commercially very successful.

### 3. Current Applications

#### 3.1. RF Filters

SAW devices are widely used for signal filtering in the field of telecommunication. To meet the current requirements, filters must have a large enough passband, which can be adjusted with a suitable IDT design. In this perspective, as for unidirectional IDTs, an appropriate design can generate specific filter templates [4]. Beyond that, much attention has also been paid to filter configurations that smartly combine several one-port SAW resonators, as impedance elements, with different topologies such as interdigitated interdigital transducer SAW (IIDT), double-mode SAW (DMS), or ladder-type [41]. The ladder-type filter is a very common configuration of such low-loss coupled SAW, represented in Figure 9, which consists of cascaded multiple stages, each one based on two SAW resonators connected in series and in parallel. Coupling them by matching the resonance frequency of a serial resonator with the antiresonance frequency of the parallel one results in a bandpass filter centered on this frequency. Such filters exhibit a relatively flat passband with low loss and good rejection of out-of-band noise [30]. Similarly, a design coupling identical SAW

resonators in double symmetric and antisymmetric modes by inverting their electrical connections can result in a wider passband filter [30,42].

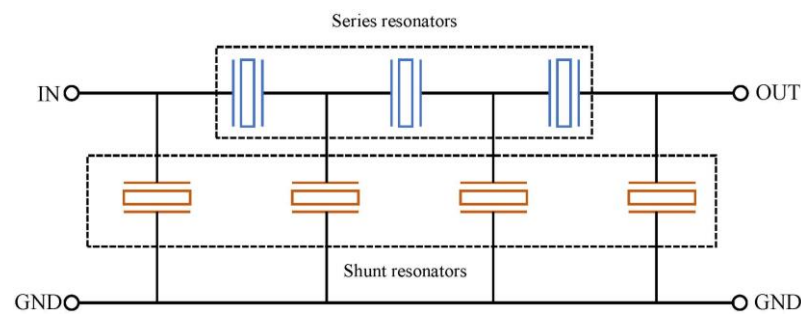


**Figure 9.** Ladder-type configuration filter for BAW and 1-port SAW devices.

There are some important properties to characterize a SAW filter:

(1) The minimum insertion loss ( $S_{21}$  parameter), quantifying the power dissipation caused by the device access, which depends on the input/output impedances of the device itself and of the input and output circuits. In case of unmatching, calibration tests are used to post-process the measurement results. Acoustic propagation can also participate in losses.

(2) The center frequency, the arithmetic average of the two cut-off frequency values,  $-3$  dB or half-power of the minimum insertion loss level.

(3) The nominal frequency range, which is the usable bandwidth over which signal transmission is observed, defined as the range between the two cut-off frequencies.

(4) The out-of-band rejection, the ratio of signals inside and outside the passband, which is defined as the drop-off value between the edge of the passband and the maximum value of the stopband.

(5) The Q value determines the maximum intrinsic bandwidth of a filter; it corresponds to the ratio of its center frequency to its 3 dB bandwidth.

With the rapid development of 5G technology, RF filters with a high frequency and Q value become increasingly in demand in the mobile phone industry as well as with new growth opportunities. This context gives RF SAW filters a significant market prospect. From the report “Surface Acoustic Wave Filter Market” by Persistence Market Research, the global SAW filter market registered a compound annual growth rate (CAGR) of 7.5% between 2015 and 2020, and was expected to reach USD 5 billion in 2021 with a CAGR of 9% by 2031. Over 50% of the market is shared by American and Japanese companies, such as Qualcomm Technologies, Qorvo, Skyworks Solutions, Microchip Technologies, and Murata Manufacturing [43,44].

Like SAW, BAW devices, currently increasingly of FBAR type, are also fundamental components for RF filters, requiring a wide bandwidth with low insertion loss and a stopband enabling the suppression of unwanted signals. Similarly, as for the SAW components, the ladder-type filters are also commonly used due to advantages such as easy design, steep filtering effect, cost, etc. Some communication systems mix ladder filters and lattice ones, in which shunt elements are diagonally crossed, to achieve a good selectivity of frequency bands with steeper filtering response [26,45]. Since the resonance frequency of SAW mainly depends on the spatial periodicity of IDTs, which is limited by lithography and patterning technology, it is quite difficult for SAW to operate above 2 GHz [46], so FBARs usually dominate the market for filters above 2.5 GHz. This is further reinforced with the 5G New Radio (NR) systems, since a main feature is the use of high-frequency millimeter wave (mmWave) and sub-6 GHz bands [47]. As a consequence, the operating frequency band will continue to expand to high frequencies, and the working bandwidth will also increase, which can be supported by the newest FBAR-based BAW technologies.

As a result, the market for filters is expected to grow explosively. Among them, the growth of BAW filters is the fastest. Indeed, the demand for connected devices, such as

vehicles, is leading to the new adoption of interface standards such as Wi-Fi, and BAW filters can also be used to establish a mobile connection with a network to enable a next-generation driving experience. The applications extend not only to the consumer electronics and automotive industries, but also to aerospace, defense, environment and industry, etc. These broad industrial applications provide prospects for significant and stable growth to the BAW filter market, which was estimated at USD 4.1 billion in 2020. By 2027, the global market for BAW filters is expected to reach USD 13 billion with a CAGR of 18% [48]. In terms of regional analysis, according to Maximize Market Research, Asia-Pacific has the largest market share and will continue to hold it in the future; Asian countries such as China, India, South Korea, and Japan are also the main consumers, and China holds the most important part due to its mature semiconductor manufacturing, telecommunications, and electronics industries [49]. The top five manufacturers in the BAW filter market are Avago Technologies (USA), Qorvo (USA), TDK (Japan), Skywork Solutions (USA), and Akoustis Technologies (USA) [49].

### 3.2. Physical Sensors and Actuators

Beside the filtering application, SAW and BAW devices are also widely used as sensors and different configurations have been developed for various physical monitoring. Among them, the QCM has been used as a way of real-time monitoring of thin film deposition thickness in microelectronics such as for evaporation equipment, based on mass-effect, with a resolution in the order of  $\text{ng}\cdot\text{cm}^{-2}$  [50]. Many other applications have been studied, such as magnetic field [51], pressure and temperature [52], acceleration [53], tire-road friction [54], and gyroscopes [55], in many sectors including automobile, consumer, etc. [56]. In addition, SAW devices are also reported as motors and actuators [57].

A SAW resonator with a delay line is reported as a highly sensitive magnetic-field sensor by several studies [58–60]. For example, Meyer et al. [58] reported a thin-film-based SAW magnetic-field sensor with a limit detection of  $2.4 \text{ nT}/\sqrt{\text{Hz}}$  at 10 Hz and  $72 \text{ pT}/\sqrt{\text{Hz}}$  at 10 kHz. This magnetic-field sensor is composed of an AlScN piezoelectric layer, AlCu IDTs, a  $\text{SiO}_2$  smoothing (guiding) layer, and a magnetostrictive FeCoSiB film deposited on the delay-layer area. In the study of Schmalz et al. [60], a multimode Love-wave SAW magnetic-field sensor was designed and the first- and second-order Love-wave modes showed sufficient sensitivity. This sensor is composed of an ST-cut quartz as the piezoelectric layer, a  $\text{SiO}_2$  layer, and a magnetostrictive  $(\text{Fe}_{90}\text{Co}_{10})_{78}\text{Si}_{12}\text{B}_{10}$  film on the delay-line area. The BAW-based magnetic-field sensor is less used, but some designs and simulations of the BAW-based magnetic-field sensor are reported [61,62].

SAW devices are also good candidates for pressure and temperature sensing [63–66]. In the Rodríguez-Madrid et al. [66] study, a SAW-based pressure sensor was reported with a sensitivity of 0.33 MHz/bar, a working frequency between 10 to 14 GHz with high-order harmonic acoustic modes. It is a one-port resonator with AlN as the piezoelectric layer deposited on a free-standing nanocrystalline diamond (NCD) layer. Müller et al. [65] reported a SAW-based temperature sensor with a sensitivity higher than 300 kHz/ $^{\circ}\text{C}$  with an operating frequency around 5.4 GHz. It is a GaN-based SAW sensor; the detection of temperature is realized by tracking resonance frequency changes as a function of temperature. Many other studies have also reported SAW- and BAW-based sensors for high temperature detection, suitable for operation in harsh environments [67–69].

At the same time, SAW-based mechanical sensors are widely used in the automotive industry, with applications such as acceleration, tire-road friction sensors, etc. In this case, a wireless readout is often used as very useful facility [52,56]. For example, Wen et al. [53] reported a SAW-based acceleration sensor with a sensitivity of 29.7 kHz/g. It is a two-port SAW device with an operating frequency of 300 MHz and a very good temperature compensation system achieved by using a metal package base. SAW sensors are also used for tire pressure and tire-road friction in car and truck tires as illustrated in this study [54]. A continuous monitoring of tire pressure, which can be reduced to 50 mBar, is achieved to estimate the riding conditions (for example with braking maneuvers, over a curbstone, etc.).

SAW devices have also been well-investigated as gyroscopes for several decades [70]. For example, a standing-wave-type SAW gyroscope was proposed by Kurosawa et al. [71]. This design was then confirmed by Varadan et al. [72] with experimental results. A two-delay-line SAW micro rate gyroscope was then proposed by Lee et al. [73]. Another progressive-waves-type SAW gyroscope was proposed by Oh et al. [74,75].

Besides such physical sensing applications, SAW devices can also serve as motors and actuators [57]. For example, Kurosawa et al. [76,77] proposed a Rayleigh-type SAW-based motor with an operating frequency near 10 MHz. It is a two-port SAW device with a delay line; a preloaded slider is placed on the wave propagation path and is driven by the frictional force. In addition, SAW devices are also widely used in microfluidic actuation and micro-object manipulation [78], based on travelling or standing waves between two sets of IDTs. Leaky-type travelling waves are usually used for actuation and manipulation, and Lamb-type standing waves are used for micro-actuators [79].

### 3.3. Biochemical Sensors

Apart from physical sensors, biochemical sensing has become a popular research topic, and a great deal of work has been carried out related to such applications of SAW and BAW for gas and liquid media [80]. Currently, such sensors can show a sensitivity with detection limits down to the ppb range [81], and SAW devices also receive intense attention in biosensing for their high sensitivity, high efficiency with label-free detection, real-time monitoring, and relatively low cost [82,83]. The sensitivity is a key factor characterizing the SAW sensor's performance [52], often improved with a sensitive layer deposited on the acoustic propagation path, which is supposed to immobilize or interact specifically with target molecules. As the acoustic wave propagation is perturbed, both the resonance frequency and the minimum loss (typically  $S_{21}$  attenuation for a two-port SAW device such as a delay-line device) are modified due to an additional mass or viscoelastic property changes at the near surface. By tracking  $S_{21}$  attenuation, resonance frequency shift, and phase, various vapors or liquids with different concentrations can be distinguished. Additional information on the real-time behavior of the adjacent medium can even be extracted from the electrical characterization out of acoustic resonance or on the reflection parameters [29].

Indeed, in 1979, Wohltjen and Dessy [84,85] first demonstrated the application and possibility of chemical/gas sensors based on SAW devices. Since then, by depositing different sensitive layers, SAW device-based gas sensors have been developed for detection of  $H_2$  [86],  $H_2S$  [87,88],  $NO_2$  [89,90],  $CO_2$  [89],  $CH_4$  [91],  $SO_2$  [92],  $NH_3$  [93],  $O_3$  [94],  $O_2$  [95],  $CO$  [96], volatile organic compounds (VOCs) [97–99], explosives [100,101], etc. In 2022, Singh et al. [102] reported a SAW-based particulate matter (PM<sub>2.5</sub>) sensor which is wearable and shows a high detection sensitivity. Another important advantage of SAW device-based sensors is that they are passive components with the potential to be interrogated wirelessly. Indeed, by using antennas, acoustic waves can be excited and received by RF electromagnetic signals. This allows SAW-based gas sensors to work in high-temperature, high-pressure, and toxic environments. Wen et al. [103] reported such a wireless SAW gas sensor with Teflon AF as a sensitive layer for  $CO_2$  detection; they reported a sensitivity in phase shift of  $1.98^\circ/ppm$ . Later, Lim et al. [89] developed a remotely controlled SAW sensor for the detection of  $CO_2$  and  $NO_2$  with simultaneous temperature measurement. The sensitive layers for  $CO_2$  and  $NO_2$  are Teflon AF and indium tin oxide, and the sensitivities are  $2.12^\circ/ppm$  and  $51.5^\circ/ppm$ , respectively. Xu et al. [104] developed a wireless SAW sensor for organophosphorus compound detection; the sensor exhibits good linearity and repeatability, and a sensitivity of  $20.1^\circ/(mg/m^3)$ .

Apart from applications in a gaseous environment, SAW-based sensors are also widely used in the liquid phase. In this case, they mostly involve waves horizontally polarized, as vertical components suffer from fast attenuation in the liquid phase, and SAW Love-mode is actually well-investigated for its high sensitivity of detection, especially in liquid [105]. Among important applications of such biosensors is the detection of deoxyribonucleic acid

(DNA). Y. Hur et al. [106] reported a 15-meroligonucleotide DNA sensor in liquid solutions with a sensitivity reaching 155 ng/mL/Hz. Kim et al. [107] reported a DNA sensor with a low detection limit of 1 ng/mL and rapid response; this sensor has the potential to be used in wireless mode. Zhang et al. [108] developed a DNA sensor with a sensitive layer of deoxy-nucleoside transferase in order to increase the phase shift, thus lowering the detection limit down to 0.8 pM. Cai et al. [109] reported a DNA sensor with a high-order harmonic acoustic mode; the sensitivity can reach  $6.7 \times 10^{-16}$  g/cm<sup>2</sup> for target DNA. SAW devices are also used for protein detection. Agostini et al. [110] developed a biosensor targeting the Streptavidin protein and the detection limit is down to sub-nanomolar,  $104 \times 10^{-12}$ . M. Choi et al. [111] developed a SAW sensor for cardiac troponin I; the detection limit is down to 24.3 pg/mL. Zhang et al. reported a carcinoembryonic antigen (CEA) biosensor; the sensitivity was reinforced by injecting a gold staining solution, allowing a detection limit down to 1 ng/mL. Jandas et al. [112] also reported a CEA sensor; the delay-line area was coated with gold and immobilized self-assembled monolayers (SAMs) of anti-CEA antibodies. The detection limit is down to 0.31 ng/mL. They later improved their sensor with a nanomaterial thin-film bioreceptor and the detection limit reached down to 0.084 ng/mL [113]. Apart from the detection of proteins, Brugger et al. [114] reported the use of SAW for monitoring the formation of neural networks and some investigation for real-time monitoring of living matter, such as organoids or other biomaterials, along with the addition that innovative nanodrugs for efficiency and/or toxicity evaluation can also be imagined [115]. Since the COVID-19 pandemic began, some SAW-based sensors for COVID virus detection have also been reported [116,117].

Similarly, BAW devices are also widely used as chemical and biological sensors, firstly based on the classical QCM, and taking into account surrounding physical parameters such as temperature and pressure, as previously described. Its operating frequency can reach up to tens of MHz and thickness-shear mode (TSM) is mostly studied [86]. With similar advantages to SAW devices but a lower frequency, some commercial products based on QCM allowed use for a large number of applications involving mass change measurements at the nanoscale resolution. Moreover, the addition of dissipation monitoring, known as "QCM-D", allows an improved characterization of both mass and viscoelastic properties changes of the medium driven at the near surface [118]. With the rapid development of BAW devices, the FBAR is also becoming a popular topic due to its good sensitivity with a higher operating frequency ranging from several to tens of GHz. The detection field includes mass pressure, gas, liquid, chemical/biosensor, etc. [119] For example, Chen et al. [120] developed a ZnO-based FBAR as a gravimetric DNA biosensor with a working frequency of 1.67 GHz. As for SAW sensors, a sensitive layer is deposited onto the top electrode of the device and the absorbed target compounds interfere with the generation and propagation of the acoustic waves. Again, since the vertical deformation is strongly attenuated into an adjacent liquid medium, a thickness-shear-mode resonator (TSM) is usually preferred for biochemical sensing applications [121].

Since the FBAR is a one-port device, detection typically consists in tracking the attenuation changes as well as the frequency or phase shift of the  $S_{11}$  parameter at the resonance [120]. The detection is also based on mechanical effects, among them the mass loading effect. Compared to the SAW sensor, whose operating frequency is typically in the range of one hundred MHz to GHz, the operating frequency of the FBAR sensor is usually in the range of sub-GHz to about 10 GHz due to the wave confinement in a very thin layer, which provides the FBAR sensor with a high sensitivity. However, a high Q factor should be ensured to accurately detect small frequency shifts.

In the field of gas sensing, Lin et al. [122] developed an FBAR-based sensor exhibiting a high sensitivity for trinitrotoluene (TNT) and 1,3,5-trinitro-1,3,5-triazacyclohexane (RDX). The detection of hydrogen (H<sub>2</sub>), carbon monoxide (CO), and ethanol vapors was also reported by Benetti et al. [123], with detection limits of 2 ppm, 40 ppm, and 500 ppm, respectively. Coupling an FBAR-based sensor with a micro-preconcentrator, Yan et al. [124] showed a high sensitivity for dimethyl methyl phosphonate (DMMP), down

to 2.64 ppm, with a fast response and a short recovery time. Zeng et al. [125] developed a temperature-compensated film bulk acoustic wave resonator (TC-FBAR) functionalized with a bilayer self-assembled poly (sodium 4-styrene-sulfonate)/poly (diallyl-dimethyl-ammonium chloride) to detect and identify volatile organic compounds (VOCs), with an interesting approach based on temperature modulation as a multiparameter virtual sensor array. Gao et al. [126] also proposed a solution for VOC identification, based on a dual transduction using mass and resistance variation of a conductive polymer, poly (3,4-ethylenedioxy-thiophene) and poly (styrene sulfonate) (PEDOT: PSS), deposited on the top of the device. The detection of 380 ppm of methanol was reported.

An FBAR device is also a good candidate for sensing in the liquid phase. As the aging of the population and disease concerns have been major topics for many decades, not to mention the impact brought by the novel coronavirus (COVID-19), biosensing technology in the liquid phase based on FBAR devices shows a wide perspective. The first FBAR-based biosensor was reported in 2003 [127]. Clear frequency shifts show DNA attachment and protein coupling. In 2004, Gabl et al. [128] reported a ZnO-based FBAR biosensor with a working frequency up to 2 GHz for the detection of DNA and protein [128]. In 2006, Weber et al. [129] showed experimentally that in the liquid phase, shear-mode FBARs have much better performance than longitudinal-mode FBARs due to higher quality factor (Q value) and lower noise level, as expected in the liquid phase. DNA sequences were also successfully detected by Zhang et al. [130], using a gold-top electrode FBAR and monitoring the shift of resonance frequency when DNA hybridization occurred. In 2011, Auer et al. reported DNA detection in a diluted serum (1%) with a resolution of 1 nM. Apart from the detection of DNA, FBAR devices have also shown their capacity to detect prostate-specific antigen (PSA), alpha-fetoprotein (AFP), and CEA [131]. Previously in 2011, Lin et al. [132] reported an FBAR sensor with a detection limit of PSA of 25 ng/cm<sup>2</sup>. Zhao et al. [133] reported a sensor of human prostate-specific antigen (hPSA) with a sensitivity of 1.5 ng/cm<sup>2</sup>. Chen et al. [134] reported a sensor of AFP with a detection limit of 1 ng/mL. Zhang et al. [131] developed a sensor of CEA, and the detection limit ranges from 0.2 to 1 mg/mL.

As we presented above, acoustic wave device (SAW and BAW)-based sensors have wide applications as physical and biochemical sensors; the market for these sensors also holds an important share. Based on the report “Acoustic Wave Sensor Market—Forecasts from 2021 to 2026” by Research and Markets, the global acoustic wave sensor market will grow from USD 836.17 million in 2019 to USD 2400.54 million in 2026, with a CAGR of 16.3%. The major players are Hawk Measurement Systems (Melbourne, Australia), NanoTemper technologies GmbH (München, Germany), Pro-micron GmbH (Kaufbeuren, Germany), Siemens (Munich, Germany), and Transense (Oxford, UK) [135].

#### 4. New Trend: Quantum Acoustics

The discussions above proposed a review of SAW and BAW devices and key applications, up to the most recent ones in terms of major trends, namely high-frequency filters and sensors. Here, we wish to give a brief introduction about a novel stream of application: quantum acoustics. Over recent decades, the research on electrons, photons, or magnetics has led a brilliant revolution in both scientific and industrial fields, and in recent times, attentions have shifted to the phonon, a quasi-particle that describes the excitation and vibration in a periodic, elastic arrangement of atoms or molecules [136]. Since most acoustic devices employ the mechanical vibrations generated from the piezoelectric effect, acoustic devices are ideal candidates to probe and control these quantum excitations in certain conditions. This is especially true for SAW devices, since their detection and sensing applications are well developed, and some examples are reported in this part.

##### 4.1. Single-Electron Probing/Controlling

With the development of semiconductor technology, current integrated circuits are composed of a huge number of transistors. In order to lower the power consumption

while improving the performance, scientists have put a large amount of effort into the field of low-dimensional electronic conductors to single-electron electronics in recent decades. Recently, SAW devices have shown good potential for single-electron probing or controlling due to their high operating frequencies and high Q value at low temperatures [137–139]. In order to detect the coupling of single-electron and SAW, a single-electron transistor (SET) is necessary [140]. Compared to classic transistors, with advantages in terms of size, voltage, and sensitivity, the SET is the most sensitive electrometer, allowing single-electron control with working temperatures in the mK range.

Gustafsson et al. [137] presented local probing of SAW for the detection of single electrons, reaching the single-phonon level at a frequency of 932 MHz. For the sample layout, a SET was placed on the propagation path of a SAW resonator, which was polarized by the piezoelectric charge when SAW passed underneath. The measurement setup was well designed and SAW were detected by their rectifying effect on the SET’s gate modulation curve. Propagating acoustic pulses with an extremely low magnitude were detected. After calculation, for each pulse, the SAW energy passing under the SET was less than a single phonon on average, which proved the possibility of single-shot phonon detection.

Other applications in single-electron controlling are also reported. For example, Takada et al. [138] reported a SAW-driven single-electron transfer with an efficiency of 99%, which can be used to perform quantum logic operations with flying electron qubits and is a significant step to efficient quantum computers. Hsiao et al. [141] used a SAW-driven lateral  $n - i - j$  junction, which operates in the single-electron limit, to generate single photons, and this electron-to-photon quantum transfer marks the first step for long-distance qubit transfer.

#### 4.2. Coherent Coupling between Magnons and Phonons

As we showed above, the coupling of photon–phonon is proven in certain conditions and some SAW-driven devices are developed for single-electron controlling. Therefore, magnetic and acoustic excitations, magnons and phonons, are also expected to interact with each other; in particular, magnons are shown to undergo a strong coupling with microwave photons [142–144]. For this reason, increasing attention is focused on coherent interactions between magnons and phonons recently [145–148].

Weiler et al. [148] demonstrated the detection of acoustic-driven ferromagnetic resonance (FMR), which shows the magnon excitation induced by SAW. Figure 10a shows the experimental setup, with a 50 nm thick polycrystalline ferromagnetic nickel film deposited on the propagating path of a SAW resonator. On Figure 10b is represented the  $S_{21}$  parameter without an applied external magnetic field; several resonances can be observed clearly and the inset highlights a 5 dB magnitude difference of the ninth harmonic resonance under two different magnetic fields. Figure 10c shows the SAW delay-line transmission parameter as a function of magnetic field strength; it exhibits a valley associated with Ni FMR, therefore proving the magnetoelastic coupling.

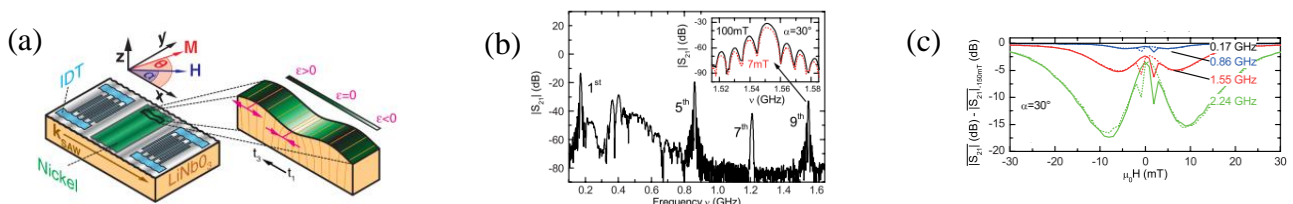


**Figure 10.** (a) Illustration of experimental setup; (b)  $S_{21}$  of the device as function of frequency when  $H = 0$  and inset focused on the influence of external magnetic field  $H$  on the 9th harmonic; (c)  $S_{21}$  as function of  $H$  for several resonance modes, adapted with permission from [148].

Recently, Zhao et al. [149] succeeded in visualizing acoustic FMR by micro-focused Brillouin light scattering ( $\mu - BLS$ ). Casals et al. [150] showed independent imaging of magnons and SAW with the synchrotron X-ray source. Besides these examples of quantum

acoustics applications, the strong coupling between magnons and phonons is still under investigation [146,151–154]. Furthermore, research in other fields continues, such as coherent coupling between phonons [155–158], coupling between elastic waves and single quantum dots [159–162], etc. These advances in quantum acoustics will likely bring a revolution in current electronics science and engineering.

## 5. Conclusions

In this review, we provided a global view about current acoustic devices. We presented the piezoelectric effect, basic structures, the acoustic theory of SAW and BAW components, and gave more details for thin-film-type BAW resonators or FBARs, which hold interesting features in terms of frequency operation and integrability compared with conventional QCM devices. We also presented the possible spurious modes and some optimized designs to reduce them and therefore improve the response. Acoustic devices have been developed over the past decades; they have proven their wide applications in communication systems. Today, with the rapid development of the fifth generation (5G) and telecommunication standards, these acoustic devices, especially FBARs, represent a broad market as RF filters, compared with conventional electromagnetic devices, thanks to much slower propagation velocity allowing for shorter wavelength and, thus, easy miniaturization and integration into circuits. We then presented another important field of applications of SAW and BAW/FBARs, namely as sensors and actuators. A section was dedicated for their application as physical sensors. Examples of their use for magnetic field, pressure, and temperature monitoring and detection were illustrated. In addition, their application in other fields such as mechanical (in automotive) and orientation measurements were presented. Some examples of SAW-based motors and actuators were also introduced. We then focused on SAW/BAW-based biochemical sensors, which are receiving increasing attention in the research field. Indeed, because of their performances, among them a high sensitivity, a versatile feature that makes them easily functionalized for selectivity, and low cost, they are widely used for gas, liquid, bio-sensing, etc. The sensing applications are still under development, with a rising demand especially for biosensors, since health concerns are more than ever a major topic. As of now, SAW and FBAR devices show a very good capacity for sensing DNA, RNA, proteins, and a wide variety of other bio-compounds. With the COVID-19 pandemic, several biosensors based on SAW and FBAR devices are also reported for the detection of SARS-CoV-2 virus and application for living-matter monitoring is under development, which could be helpful for fast screening of therapeutic nanodrugs, for example. Lastly, we presented current trends related to quantum acoustics, which studies the behavior of phonons and their interactions, as opportunities for new schemes to control quantum information and explore atomic physics beyond photonic systems. SAW is the ideal candidate in this emerging field with interest in both fundamental and applied research.

**Author Contributions:** C.D. and H.H. planned and supervised all the work while Y.Y. wrote the main draft of review article. All authors have read and agreed to the published version of the manuscript.

**Funding:** This research was funded by CNRS grant “Excellence Science” Joint Research Program 2019. And the APC was funded by the financial support of the Agence Nationale de la Recherche (ANR) for projects CARDIF (ANR-19-CE04-0010).

**Data Availability Statement:** Not applicable.

**Conflicts of Interest:** The authors declare no conflict of interest. The funders had no role in the design of the study, in the collection, analyses, or interpretation of data, in the writing of the manuscript, or in the decision to publish the results.

## References

1. Weigel, R.; Morgan, D.P.; Owens, J.M.; Ballato, A.; Lakin, K.M.; Hashimoto, K.Y.; Ruppel, C.C. Microwave acoustic materials, devices, and applications. *IEEE Trans. Microw. Theory Tech.* **2002**, *50*, 738–749. [[CrossRef](#)]
2. Tirado, J.A.V. *Bulk Acoustic Wave Resonators and Their Application to Microwave Devices*; Universitat Autònoma de Barcelona: Barcelona, Spain, 2010.
3. Tummala, R.R. *System on Package: Miniaturization of the Entire System*; McGraw-Hill Education: New York, NY, USA, 2008.
4. Morgan, D. *Surface Acoustic Wave Filters: With Applications to Electronic Communications and Signal Processing*; Academic Press: Cambridge, MA, USA, 2010.
5. Liu, Y.; Cai, Y.; Zhang, Y.; Tovstopyat, A.; Liu, S.; Sun, C. Materials, design, and characteristics of bulk acoustic wave resonator: A review. *Micromachines* **2020**, *11*, 630. [[CrossRef](#)] [[PubMed](#)]
6. Wells, J.C. *Longman Pronunciation Dictionary (New Edition)*; Longman: Harlow, UK, 2000.
7. Curie, J.; Curie, P. Développement par compression de l'électricité polaire dans les cristaux hémihédres à faces inclinées. *Bull. De Minéralogie* **1880**, *3*, 90–93. [[CrossRef](#)]
8. Curie, J.; Curie, P. Contractions and expansions produced by voltages in hemihedral crystals with inclined faces. *Comptes Rendus* **1881**, *93*, 1137–1140.
9. Lakin, K.M. Thin film resonator technology. In Proceedings of the IEEE International Frequency Control Symposium and PDA Exhibition Jointly with the 17th European Frequency and Time Forum, 2003, Proceedings of the 2003, Tampa, FL, USA, 4–8 May 2003.
10. Wright, P. A review of SAW resonator filter technology. In *IEEE 1992 Ultrasonics Symposium Proceedings*; IEEE: Tucson, AZ, USA, 1992.
11. Makkonen, T.; Pensala, T.; Vartiainen, J.; Knuutila, J.V.; Kaitila, J.; Salomaa, M.M. Estimating materials parameters in thin-film BAW resonators using measured dispersion curves. *IEEE Trans. Ultrason. Ferroelectr. Freq. Control.* **2004**, *51*, 42–51. [[CrossRef](#)]
12. Viktorov, I.A. *Rayleigh and Lamb Waves: Physical Theory and Applications*; Plenum Press: New York, NY, USA, 1967.
13. Love, A.E.H. *Some Problems of Geodynamics: Being an Essay to which the Adams Prize in the University of Cambridge was Adjudged in 1911*; University Press: Cambridge, UK, 1911; Volume 911.
14. White, R.M.; Voltmer, F.W. Direct piezoelectric coupling to surface elastic waves. *Appl. Phys. Lett.* **1965**, *7*, 314–316. [[CrossRef](#)]
15. Newell, W. Face-mounted piezoelectric resonators. *Proc. IEEE* **1965**, *53*, 575–581. [[CrossRef](#)]
16. Sliker, T.; Roberts, D. A thin-film CdS-quartz composite resonator. *J. Appl. Phys.* **1967**, *38*, 2350–2358. [[CrossRef](#)]
17. Grudkowski, T.W.; Black, J.F.; Reeder, T.M.; Cullen, D.E.; Wagner, R.A. Fundamental-mode VHF/UHF miniature acoustic resonators and filters on silicon. *Appl. Phys. Lett.* **1980**, *37*, 993–995. [[CrossRef](#)]
18. Lakin, K.; Wang, J. Acoustic bulk wave composite resonators. *Appl. Phys. Lett.* **1981**, *38*, 125–127. [[CrossRef](#)]
19. Ruby, R. Micromachined cellular filters. In *1996 IEEE MTT-S International Microwave Symposium Digest*; IEEE: San Francisco, CA, USA, 1996.
20. Ruby, R.; Bradley, P.; Larson, J.D.; Oshmyansky, Y.J.E.L. PCS 1900 MHz duplexer using thin film bulk acoustic resonators (FBARs). *Electron. Lett.* **1999**, *35*, 794–795. [[CrossRef](#)]
21. Aigner, R. MEMS in RF filter applications: Thin-film bulk acoustic wave technology. *Sens. Update* **2003**, *12*, 175–210. [[CrossRef](#)]
22. Wang, L.-P.; Ginsburg, E.; Diamant, D.; Ma, Q.; Huang, Z.; Suo, Z. Method of fabricating multiple-frequency film bulk acoustic resonators in a single chip. In *2006 IEEE International Frequency Control Symposium and Exposition*; IEEE: Miami, FL, USA, 2006.
23. Fattinger, G.G. BAW resonator design considerations-an overview. In *2008 IEEE International Frequency Control Symposium*; IEEE: Honolulu, HI, USA, 2008.
24. Loebel, H.P.; Klee, M.; Metzmacher, C.; Brand, W.; Milsom, R.; Lok, P. Piezoelectric thin AlN films for bulk acoustic wave (BAW) resonators. *Mater. Chem. Phys.* **2003**, *79*, 146. [[CrossRef](#)]
25. Kim, E.K.; Lee, T.Y.; Jeong, Y.H.; Park, Y.; Song, J.T. Air gap type thin film bulk acoustic resonator fabrication using simplified process. *Thin Solid Film.* **2006**, *496*, 653–657. [[CrossRef](#)]
26. Zhang, Y.; Chen, D. *Multilayer Integrated Film Bulk Acoustic Resonators*; Springer Science & Business Media: Shanghai, China, 2012.
27. Villa-López, F.H.; Rughoobur, G.; Thomas, S.; Flewitt, A.J.; Cole, M.; Gardner, J.W. Design and modelling of solidly mounted resonators for low-cost particle sensing. *Meas. Sci. Technol.* **2015**, *27*, 025101. [[CrossRef](#)]
28. Hashimoto, K.-Y. *RF Bulk Acoustic Wave Filters for Communications*; Artech House: New York, NY, USA, 2009.
29. Rube, M.; Tamarin, O.; Sebelou, M.; Sadli, I.; Hallil, H.; Linguet, L.; Rebiere, D.; Dejous, C. Unconventional protocol for SAW sensor: Multi-physic response enrichment in liquid medium. *IEEE Sens. J.* **2021**, *22*, 11345–11354. [[CrossRef](#)]
30. Hashimoto, K.-y.; Hashimoto, K.-Y. *Surface Acoustic Wave Devices in Telecommunications*; Springer: Berlin/Heidelberg, Germany, 2000; Volume 116.
31. Koskela, J.; Knuutila, J.V.; Makkonen, T.; Plessky, V.P.; Salomaa, M.M. Acoustic loss mechanisms in leaky SAW resonators on lithium tantalate. *IEEE Trans. Ultrason. Ferroelectr. Freq. Control.* **2001**, *48*, 1517–1526. [[CrossRef](#)]
32. Giovannini, M.; Yazici, S.; Kuo, N.-K.; Piazza, G. Spurious mode suppression via apodization for 1 GHz AlN contour-mode resonators. In *2012 IEEE International Frequency Control Symposium Proceedings*; IEEE: Baltimore, MD, USA, 2012.
33. Bausk, E.V. Optimization of broadband withdrawal weighted interdigital transducers for high selective SAW filters. *IEEE Trans. Ultrason. Ferroelectr. Freq. Control.* **1999**, *46*, 1276–1282. [[CrossRef](#)]

34. Marshall, F.G.; Newton, C.; Paige, E. Theory and design of the surface acoustic wave multistrip coupler. *IEEE Trans. Microw. Theory Tech.* **1973**, *21*, 206–215. [CrossRef]
35. Yokoyama, T.; Nishihara, T.; Taniguchi, S.; Iwaki, M.; Satoh, Y.; Ueda, M.; Miyashita, T. New electrode material for low-loss and high-Q FBAR filters. In *IEEE Ultrasonics Symposium, 2004*; IEEE: Montreal, QC, Canada, 2004.
36. Pang, W.; Zhang, H.; Whangbo, S.; Kim, E.S. High Q film bulk acoustic resonator from 2.4 to 5.1 GHz. In *17th IEEE International Conference on Micro Electro Mechanical Systems. Maastricht MEMS 2004 Technical Digest*; IEEE: Maastricht, The Netherlands, 2004.
37. Caspers, F. RF engineering basic concepts: S-parameters. *arXiv* **2012**, arXiv:1201.2346.
38. Fattinger, G.; Marksteiner, S.; Kaitila, J.; Aigner, R. Optimization of acoustic dispersion for high performance thin film BAW resonators. In *IEEE Ultrasonics Symposium, 2005*; IEEE: Rotterdam, The Netherlands, 2005.
39. Ruby, R.; Larson, J.; Feng, C.; Fazio, S. The effect of perimeter geometry on FBAR resonator electrical performance. In *IEEE MTT-S International Microwave Symposium Digest, 2005*; IEEE: Long Beach, CA, USA, 2005.
40. Lee, J.-H.; Yao, C.-M.; Tzeng, K.-Y.; Cheng, C.-W.; Shih, Y.-C. Optimization of frame-like film bulk acoustic resonators for suppression of spurious lateral modes using finite element method. In *IEEE Ultrasonics Symposium, 2004*; IEEE: Montreal, QC, Canada, 2004.
41. World, R.W. Difference between SAW Filters Types | IIDT, DMS, Ladder Type. 2012. Available online: <https://www.rfwireless-world.com/Terminology/Difference-between-SAW-filter-types-IIDT-DMS-and-Ladder.html> (accessed on 8 December 2022).
42. Morita, T.; Watanabe, Y.; Tanaka, M.; Nakazawa, Y. Wideband low loss double mode SAW filters. In *IEEE 1992 Ultrasonics Symposium Proceedings*; IEEE: Tucson, AZ, USA, 1992.
43. PersistenceMarketResearch. Surface Acoustic Wave Filter Market 2020. Available online: <https://www.persistencemarketresearch.com/market-research/surface-acoustic-wave-filter-market.asp> (accessed on 6 December 2022).
44. Cédric, M.; Mohammed, T. Cellular RF Front-End Technologies for Mobile Handset 2021. 2021. Available online: <https://www.i-micronews.com/products/cellular-rf-front-end-technologies-for-mobile-handset-2021/> (accessed on 6 December 2022).
45. Chatras, M.; Bila, S.; Giraud, S.; Catherinot, L.; Fan, J.; Cros, D.; Aubourg, M.; Flament, A.; Frappé, A.; Stefanelli, B. Modeling and Design of BAW Resonators and Filters for Integration in a UMTS Transmitter. In *Modeling and Measurement Methods for Acoustic Waves and for Acoustic Microdevices*; InTech Rijeka: Rijeka, Croatia, 2013; pp. 323–354.
46. Aigner, R. SAW and BAW technologies for RF filter applications: A review of the relative strengths and weaknesses. In *2008 IEEE Ultrasonics Symposium*; IEEE: Beijing, China, 2008.
47. Li, Y.-N.R.; Gao, B.; Zhang, X.; Huang, K. Beam management in millimeter-wave communications for 5G and beyond. *IEEE Access* **2020**, *8*, 13282–13293. [CrossRef]
48. Researchandmarkets. Bulk Acoustic Wave (BAW) Filters-Global Market Trajectory & Analytics. 2021. Available online: <https://www.researchandmarkets.com/reports/5301638/bulk-acoustic-wave-baw-filters-global-market> (accessed on 2 December 2022).
49. Research, M.M. Global Bulk-Acoustic-Wave (BAW) Filters Market-Industry Analysis and Forecast (2019–2027)-By Type, Application, and Region. 2021. Available online: <https://www.maximizemarketresearch.com/market-report/global-bulk-acoustic-wave-baw-filters-market/69367/> (accessed on 6 December 2022).
50. Ramadan, B.; Piyakis, K.; Kos, J. High accuracy quartz crystal thin film monitor. *Rev. Sci. Instrum.* **1979**, *50*, 867–871. [CrossRef] [PubMed]
51. Yang, Y.; Mengue, P.; Mishra, H.; Floer, C.; Hage-Ali, S.; Petit Watelot, S.; Lacour, D.; Hehn, M.; Han, T.; Elmazria, O. Wireless Multifunctional Surface Acoustic Wave Sensor for Magnetic Field and Temperature Monitoring. *Adv. Mater. Technol.* **2022**, *7*, 2100860. [CrossRef]
52. Hallil, H.; Dejous, C.; Hage-Ali, S.; Elmazria, O.; Rossignol, J.; Stuerger, D.; Talbi, A.; Mazzamurro, A.; Joubert, P.-Y.; Lefeuvre, E. Passive resonant sensors: Trends and future prospects. *IEEE Sens. J.* **2021**, *21*, 12618–12632. [CrossRef]
53. Wang, W.; Huang, Y.; Liu, X.; Liang, Y. Surface acoustic wave acceleration sensor with high sensitivity incorporating ST-X quartz cantilever beam. *Smart Mater. Struct.* **2014**, *24*, 015015. [CrossRef]
54. Pohl, A.; Ostermayer, G.; Reindl, L.; Seifert, F. Monitoring the tire pressure at cars using passive SAW sensors. In *1997 IEEE Ultrasonics Symposium Proceedings. An International Symposium (Cat. No. 97CH36118)*; IEEE: Toronto, ON, Canada, 1997.
55. Oh, H.; Wang, W.; Yang, S.; Lee, K. Development of SAW based gyroscope with high shock and thermal stability. *Sens. Actuators A Phys.* **2011**, *165*, 8–15. [CrossRef]
56. Hribšek, M.F.; Tošić, D.V.; Radosavljević, M.R. Surface acoustic wave sensors in mechanical engineering. *FME Trans.* **2010**, *38*, 11–18.
57. Zhang, S.-y.; Cheng, L.-p. Surface acoustic wave motors and actuators: Mechanism, structure, characteristic and application. In *Acoustic Waves*; InTech: London, UK, 2010; pp. 207–232.
58. Meyer, J.M.; Schell, V.; Su, J.; Fichtner, S.; Yarar, E.; Niekief, F.; Giese, T.; Kittmann, A.; Thormählen, L.; Lebedev, V. Thin-Film-Based SAW Magnetic Field Sensors. *Sensors* **2021**, *21*, 8166. [CrossRef]
59. Durdaut, P.; Müller, C.; Kittmann, A.; Schell, V.; Bahr, A.; Quandt, E.; Knöchel, R.; Höft, M.; McCord, J. Phase Noise of SAW Delay Line Magnetic Field Sensors. *Sensors* **2021**, *21*, 5631. [CrossRef]
60. Schmalz, J.; Kittmann, A.; Durdaut, P.; Spetzler, B.; Faupel, F.; Höft, M.; Quandt, E.; Gerken, M. Multi-mode love-wave SAW magnetic-field sensors. *Sensors* **2020**, *20*, 3421. [CrossRef]
61. Ren, W.; Li, J.; Liu, G.; Chen, J.; Chen, S.; Gu, Z.; Li, J.; Li, J.; Gao, Y. Design and Optimization of a BAW Magnetic Sensor Based on Magnetoelectric Coupling. *Micromachines* **2022**, *13*, 206. [CrossRef] [PubMed]

62. Chen, S.; Ren, W.-C.; Li, J.; Peng, C.-r.; Gao, Y. Modeling of magnetic sensor based on BAW magnetoelectric coupling micro-heterostructure. In *2021 IEEE 16th International Conference on Nano/Micro Engineered and Molecular Systems (NEMS)*; IEEE: Xiamen, China, 2021.
63. Gao, X.; Cheng, L.; Xue, X.; Zhai, S.; Liang, Y.; Wang, W.; Liu, M.; Zhu, J.; Li, Z. Development of Wireless and Passive SAW Temperature Sensor with Very High Accuracy. *Appl. Sci.* **2021**, *11*, 7422. [[CrossRef](#)]
64. Nicolay, P.; Chambon, H.; Bruckner, G.; Gruber, C.; Ballandras, S.; Courjon, E.; Stadler, M. A LN/Si-based SAW pressure sensor. *Sensors* **2018**, *18*, 3482. [[CrossRef](#)] [[PubMed](#)]
65. Müller, A.; Konstantinidis, G.; Buiculescu, V.; Dinescu, A.; Stavrinidis, A.; Stefanescu, A.; Stavrinidis, G.; Giangu, I.; Cismaru, A.; Modoveanu, A. GaN/Si based single SAW resonator temperature sensor operating in the GHz frequency range. *Sens. Actuators A Phys.* **2014**, *209*, 115–123. [[CrossRef](#)]
66. Rodríguez-Madrid, J.; Iriarte, G.; Williams, O.A.; Calle, F. High precision pressure sensors based on SAW devices in the GHz range. *Sens. Actuators A Phys.* **2013**, *189*, 364–369. [[CrossRef](#)]
67. Yu, F.; Zhang, S.; Zhao, X.; Yuan, D.; Qin, L.; Wang, Q.-m.; Shrout, T.R. Investigation of Ca<sub>3</sub>TaGa<sub>3</sub>Si<sub>2</sub>O<sub>14</sub> piezoelectric crystals for high temperature sensors. *J. Appl. Phys.* **2011**, *109*, 114103. [[CrossRef](#)]
68. Chiu, K.-H.; Chen, H.-R.; Huang, S.R.-S. High-performance film bulk acoustic wave pressure and temperature sensors. *Jpn. J. Appl. Phys.* **2007**, *46*, 1392. [[CrossRef](#)]
69. Mansfeld, G.; Alekseev, S.; Kotelyansky, I.; Kirillov, A.; Veretin, V. BAW microwave temperature sensor. In *Sensors, 2004 IEEE*; IEEE: Vienna, Austria, 2004.
70. Oh, H.; Lee, K.J.; Lee, K.; Yang, S.S. Gyroscopes based on surface acoustic waves. *Micro Nano Syst. Lett.* **2015**, *3*, 1–10. [[CrossRef](#)]
71. Kurosawa, M.; Fukuda, Y.; Takasaki, M.; Higuchi, T. A surface-acoustic-wave gyro sensor. *Sens. Actuators A Phys.* **1998**, *66*, 33–39. [[CrossRef](#)]
72. Varadan, V.; Suh, W.; Xavier, P.; Jose, K.; Varadan, V. Design and development of a MEMS-IDT gyroscope. *Smart Mater. Struct.* **2000**, *9*, 898. [[CrossRef](#)]
73. Lee, S.W.; Rhim, J.W.; Park, S.W.; Yang, S.S. A micro rate gyroscope based on the SAW gyroscopic effect. *J. Micromechanics Microengineering* **2007**, *17*, 2272. [[CrossRef](#)]
74. Oh, H.; Yang, S.; Lee, K. Development of surface acoustic wave-based microgyroscope utilizing progressive wave. *Jpn. J. Appl. Phys.* **2010**, *49*, 06GN16. [[CrossRef](#)]
75. Oh, H.; Lee, K.; Yang, S.S.; Wang, W. Enhanced sensitivity of a surface acoustic wave gyroscope using a progressive wave. *J. Micromechanics Microengineering* **2011**, *21*, 075015. [[CrossRef](#)]
76. Kurosawa, M.; Takahashi, M.; Higuchi, T. Friction drive surface acoustic wave motor. *Ultrasonics* **1996**, *34*, 243–246. [[CrossRef](#)]
77. Kurosawa, M.K.; Itoh, H.; Asai, K. Elastic friction drive of surface acoustic wave motor. *Ultrasonics* **2003**, *41*, 271–275. [[CrossRef](#)]
78. Destgeer, G.; Sung, H.J. Recent advances in microfluidic actuation and micro-object manipulation via surface acoustic waves. *Lab A Chip* **2015**, *15*, 2722–2738. [[CrossRef](#)]
79. Mazalan, M.B.; Noor, A.M.; Wahab, Y.; Yahud, S.; Zaman, W.S.W.K. Current Development in Interdigital Transducer (IDT) Surface Acoustic Wave Devices for Live Cell In Vitro Studies: A Review. *Micromachines* **2021**, *13*, 30. [[CrossRef](#)]
80. Pohl, A. A review of wireless SAW sensors. *IEEE Trans. Ultrason. Ferroelectr. Freq. Control.* **2000**, *47*, 317–332. [[CrossRef](#)]
81. Panneerselvam, G.; Thirumal, V.; Pandya, H.M. Review of surface acoustic wave sensors for the detection and identification of toxic environmental gases/vapours. *Arch. Acoust.* **2018**, *43*, 357–367.
82. Zida, S.I.; Lin, Y.D.; Khung, Y.L. Current Trends on Surface Acoustic Wave Biosensors. *Adv. Mater. Technol.* **2021**, *6*, 2001018. [[CrossRef](#)]
83. Dejous, C.; Hallil, H.; Raimbault, V.; Lachaud, J.-L.; Plano, B.; Delépée, R.; Favetta, P.; Agrofoglio, L.; Rebière, D. Love acoustic wave-based devices and molecularly-imprinted polymers as versatile sensors for electronic nose or tongue for cancer monitoring. *Sensors* **2016**, *16*, 915. [[CrossRef](#)] [[PubMed](#)]
84. Wohltjen, H.; Dessy, R. Surface acoustic wave probe for chemical analysis. I. Introduction and instrument description. *Anal. Chem.* **1979**, *51*, 1458–1464. [[CrossRef](#)]
85. Wohltjen, H.; Dessy, R. Surface acoustic wave probes for chemical analysis. II. Gas chromatography detector. *Anal. Chem.* **1979**, *51*, 1465–1470. [[CrossRef](#)]
86. Sil, D.; Hines, J.; Udeoyo, U.; Borguet, E. Palladium nanoparticle-based surface acoustic wave hydrogen sensor. *ACS Appl. Mater. Interfaces* **2015**, *7*, 5709–5714. [[CrossRef](#)] [[PubMed](#)]
87. Luo, W.; Fu, Q.; Zhou, D.; Deng, J.; Liu, H.; Yan, G. A surface acoustic wave H<sub>2</sub>S gas sensor employing nanocrystalline SnO<sub>2</sub> thin film. *Sens. Actuators B Chem.* **2013**, *176*, 746–752. [[CrossRef](#)]
88. Asad, M.; Sheikhi, M.H. Surface acoustic wave based H<sub>2</sub>S gas sensors incorporating sensitive layers of single wall carbon nanotubes decorated with Cu nanoparticles. *Sens. Actuators B Chem.* **2014**, *198*, 134–141. [[CrossRef](#)]
89. Lim, C.; Wang, W.; Yang, S.; Lee, K. Development of SAW-based multi-gas sensor for simultaneous detection of CO<sub>2</sub> and NO<sub>2</sub>. *Sens. Actuators B Chem.* **2011**, *154*, 9–16. [[CrossRef](#)]
90. Thomas, S.; Cole, M.; De Luca, A.; Torrisi, F.; Ferrari, A.; Udrea, F.; Gardner, J.W. Graphene-coated Rayleigh SAW resonators for NO<sub>2</sub> detection. *Procedia Eng.* **2014**, *87*, 999–1002. [[CrossRef](#)]
91. Wang, W.; Hu, H.; Liu, X.; He, S.; Pan, Y.; Zhang, C.; Dong, C. Development of a room temperature SAW methane gas sensor incorporating a supramolecular cryptophane a coating. *Sensors* **2016**, *16*, 73. [[CrossRef](#)] [[PubMed](#)]

92. Lee, Y.; Kim, H.; Roh, Y.; Cho, H.; Baik, S. Development of a SAW gas sensor for monitoring SO<sub>2</sub> gas. *Sens. Actuators A Phys.* **1998**, *64*, 173–178. [[CrossRef](#)]
93. Tang, Y.-L.; Li, Z.-J.; Ma, J.-Y.; Guo, Y.-J.; Fu, Y.-Q.; Zu, X.-T. Ammonia gas sensors based on ZnO/SiO<sub>2</sub> bi-layer nanofilms on ST-cut quartz surface acoustic wave devices. *Sens. Actuators B Chem.* **2014**, *201*, 114–121. [[CrossRef](#)]
94. Westafer, R.S.; Levitin, G.; Hess, D.W.; Bergin, M.H.; Hunt, W.D. Detection of ppb ozone using a dispersive surface acoustic wave reflective delay line with integrated reference signal. *Sens. Actuators B Chem.* **2014**, *192*, 406–413. [[CrossRef](#)]
95. Zheng, P.; Chin, T.-I.; Greve, D.; Oppenheim, I.; Malone, V.; Cao, L. High-temperature langasite SAW oxygen sensor. *IEEE Trans. Ultrason. Ferroelectr. Freq. Control.* **2011**, *58*, 1538–1540. [[CrossRef](#)] [[PubMed](#)]
96. Sadek, A.; Wlodarski, W.; Shin, K.; Kaner, R.B.; Kalantar-zadeh, K. A layered surface acoustic wave gas sensor based on a polyaniline/In<sub>2</sub>O<sub>3</sub> nanofibre composite. *Nanotechnology* **2006**, *17*, 4488. [[CrossRef](#)]
97. Reichert, J.; Coerdts, W.; Ache, H. Development of a surface acoustic wave sensor array for the detection of methanol in fuel vapours. *Sens. Actuators B Chem.* **1993**, *13*, 293–296. [[CrossRef](#)]
98. Tang, K.-T.; Li, C.-H.; Chiu, S.-W. An electronic-nose sensor node based on a polymer-coated surface acoustic wave array for wireless sensor network applications. *Sensors* **2011**, *11*, 4609–4621. [[CrossRef](#)] [[PubMed](#)]
99. Wang, Y.; Du, X.; Long, Y.; Tang, X.; Chen, Z.; Jiang, Y. Real-time detection of styrene using SAW sensors based on hexafluoroisopropanol group functionalized hydrogen-bond acidic polymers. *Sens. Actuators B Chem.* **2015**, *206*, 252–257. [[CrossRef](#)]
100. Houser, E.J.; Mlsna, T.E.; Nguyen, V.K.; Chung, R.; Mowery, R.L.; McGill, R.A. Rational materials design of sorbent coatings for explosives: Applications with chemical sensors. *Talanta* **2001**, *54*, 469–485. [[CrossRef](#)]
101. Kannan, G.; Nimal, A.; Mittal, U.; Yadava, R.; Kapoor, J. Adsorption studies of carbowax coated surface acoustic wave (SAW) sensor for 2, 4-dinitro toluene (DNT) vapour detection. *Sens. Actuators B Chem.* **2004**, *101*, 328–334. [[CrossRef](#)]
102. Singh, G.; Kim, S.; Lee, K. Development of a highly sensitive and portable particulate matter SAW sensor and interface electronics. *Sens. Actuators A Phys.* **2022**, *343*, 113641. [[CrossRef](#)]
103. Wang, W.; Lee, K.; Kim, T.; Park, I.; Yang, S. A novel wireless, passive CO<sub>2</sub> sensor incorporating a surface acoustic wave reflective delay line. *Smart Mater. Struct.* **2007**, *16*, 1382. [[CrossRef](#)]
104. Xu, F.-Q.; Wang, W.; Xue, X.-F.; Hu, H.-L.; Liu, X.-L.; Pan, Y. Development of a wireless and passive SAW-based chemical sensor for organophosphorous compound detection. *Sensors* **2015**, *15*, 30187–30198. [[CrossRef](#)] [[PubMed](#)]
105. Länge, K.; Rapp, B.E.; Rapp, M. Surface acoustic wave biosensors: A review. *Anal. Bioanal. Chem.* **2008**, *391*, 1509–1519. [[CrossRef](#)] [[PubMed](#)]
106. Hur, Y.; Han, J.; Seon, J.; Pak, Y.E.; Roh, Y. Development of an SH-SAW sensor for the detection of DNA hybridization. *Sens. Actuators A Phys.* **2005**, *120*, 462–467. [[CrossRef](#)]
107. Kim, S.-G.; Lee, H.-J.; Lee, J.-H.; Jung, H.-I.; Yook, J.-G. A highly sensitive and label free biosensing platform for wireless sensor node system. *Biosens. Bioelectron.* **2013**, *50*, 362–367. [[CrossRef](#)] [[PubMed](#)]
108. Zhang, Y.; Yang, F.; Sun, Z.; Li, Y.-T.; Zhang, G.-J. A surface acoustic wave biosensor synergizing DNA-mediated in situ silver nanoparticle growth for a highly specific and signal-amplified nucleic acid assay. *Analyst* **2017**, *142*, 3468–3476. [[CrossRef](#)] [[PubMed](#)]
109. Cai, H.-L.; Yang, Y.; Chen, X.; Mohammad, M.A.; Ye, T.-X.; Guo, C.-R.; Yi, L.-T.; Zhou, C.-J.; Liu, J.; Ren, T.-L. A third-order mode high frequency biosensor with atomic resolution. *Biosens. Bioelectron.* **2015**, *71*, 261–268. [[CrossRef](#)]
110. Agostini, M.; Greco, G.; Cecchini, M. A Rayleigh surface acoustic wave (R-SAW) resonator biosensor based on positive and negative reflectors with sub-nanomolar limit of detection. *Sens. Actuators B Chem.* **2018**, *254*, 1–7. [[CrossRef](#)]
111. Choi, Y.-S.; Lee, J.; Lee, Y.; Kwak, J.; Suk Lee, S. Increase in detection sensitivity of surface acoustic wave biosensor using triple transit echo wave. *Appl. Phys. Lett.* **2018**, *113*, 083702. [[CrossRef](#)]
112. Jandas, P.; Luo, J.; Quan, A.; Qiu, C.; Cao, W.; Fu, C.; Fu, Y.Q. Highly selective and label-free Love-mode surface acoustic wave biosensor for carcinoembryonic antigen detection using a self-assembled monolayer bioreceptor. *Appl. Surf. Sci.* **2020**, *518*, 146061. [[CrossRef](#)]
113. Jandas, P.; Luo, J.; Prabakaran, K.; Chen, F.; Fu, Y.Q. Highly stable, love-mode surface acoustic wave biosensor using Au nanoparticle-MoS<sub>2</sub>-rGO nano-cluster doped polyimide nanocomposite for the selective detection of carcinoembryonic antigen. *Mater. Chem. Phys.* **2020**, *246*, 122800. [[CrossRef](#)]
114. Brugger, M.S.; Grunden, S.; Doyle, A.; Theogarajan, L.; Wixforth, A.; Westerhausen, C. Orchestrating cells on a chip: Employing surface acoustic waves towards the formation of neural networks. *Phys. Rev. E* **2018**, *98*, 012411. [[CrossRef](#)] [[PubMed](#)]
115. Dejous, C.; Hallil, H.; Raimbault, V.; Rukkumani, R.; Yakhmi, J.V. Using microsensors to promote the development of innovative therapeutic nanostructures. In *Nanostructures for Novel Therapy*; Elsevier: Amsterdam, The Netherlands, 2017; pp. 539–566.
116. Peng, Y.-C.; Cheng, C.-H.; Yatsuda, H.; Liu, S.-H.; Liu, S.-J.; Kogai, T.; Kuo, C.-Y.; Wang, R.Y. A novel rapid test to detect Anti-SARS-CoV-2 N protein IgG based on shear horizontal surface acoustic wave (SH-SAW). *Diagnostics* **2021**, *11*, 1838. [[CrossRef](#)] [[PubMed](#)]
117. Kumar, M.; Bhadu, D. Design performance and frequency response analysis of SAW-based sensor for dichloromethane gas sensing amidst the COVID-19. *J. Vib. Eng. Technol.* **2021**, *9*, 725–732. [[CrossRef](#)]
118. Edvardsson, M. What Is QCM-D? 2020. Available online: <https://www.biolinscientific.com/blog/what-is-qcmd> (accessed on 8 December 2022).

119. Zhang, Y.; Luo, J.; Flewitt, A.J.; Cai, Z.; Zhao, X. Film bulk acoustic resonators (FBARs) as biosensors: A review. *Biosens. Bioelectron.* **2018**, *116*, 1–15. [CrossRef] [PubMed]
120. Chen, Y.; Reyes, P.I.; Duan, Z.; Saraf, G.; Wittstruck, R.; Lu, Y.; Taratula, O.; Galoppini, E. Multifunctional ZnO-based thin-film bulk acoustic resonator for biosensors. *J. Electron. Mater.* **2009**, *38*, 1605–1611. [CrossRef]
121. Mujahid, A.; Afzal, A.; Dickert, F.L. An overview of high frequency acoustic sensors—QCMs, SAWs and FBARs—Chemical and biochemical applications. *Sensors* **2019**, *19*, 4395. [CrossRef]
122. Lin, A.; Yu, H.; Waters, M.S.; Kim, E.S.; Goodman, S.D. Explosive trace detection with FBAR-based sensor. In *2008 IEEE 21st International Conference on Micro Electro Mechanical Systems*; IEEE: Tucson, AZ, USA, 2008.
123. Benetti, M.; Cannatà, D.; Di Pietrantonio, F.; Foglietti, V.; Verona, E. Microbalance chemical sensor based on thin-film bulk acoustic wave resonators. *Appl. Phys. Lett.* **2005**, *87*, 173504. [CrossRef]
124. Yan, X.; Qu, H.; Chang, Y.; Pang, W.; Duan, X. A prototype portable instrument employing micro-preconcentrator and FBAR sensor for the detection of chemical warfare agents. *Nanotechnol. Precis. Eng.* **2022**, *5*, 013005. [CrossRef]
125. Zeng, G.; Wu, C.; Chang, Y.; Zhou, C.; Chen, B.; Zhang, M.; Li, J.; Duan, X.; Yang, Q.; Pang, W. Detection and discrimination of volatile organic compounds using a single film bulk acoustic wave resonator with temperature modulation as a multiparameter virtual sensor array. *ACS Sens.* **2019**, *4*, 1524–1533. [CrossRef]
126. Gao, F.; Xuan, W.; Bermak, A.; Boussaid, F.; Tsui, C.-Y.; Luo, J. Dual transduction on a single sensor for gas identification. *Sens. Actuators B Chem.* **2019**, *278*, 21–27. [CrossRef]
127. Gabl, R.; Green, E.; Schreiter, M.; Feucht, H.; Zeininger, H.; Primig, R.; Pitzer, D.; Eckstein, G.; Wersing, W. Novel integrated FBAR sensors: A universal technology platform for bio-and gas-detection. In *SENSORS, 2003 IEEE*; IEEE: Piscataway, NJ, USA, 2003.
128. Gabl, R.; Feucht, H.-D.; Zeininger, H.; Eckstein, G.; Schreiter, M.; Primig, R.; Pitzer, D.; Wersing, W. First results on label-free detection of DNA and protein molecules using a novel integrated sensor technology based on gravimetric detection principles. *Biosens. Bioelectron.* **2004**, *19*, 615–620. [CrossRef] [PubMed]
129. Weber, J.; Albers, W.M.; Tuppurainen, J.; Link, M.; Gabl, R.; Wersing, W.; Schreiter, M. Shear mode FBARs as highly sensitive liquid biosensors. *Sens. Actuators A Phys.* **2006**, *128*, 84–88. [CrossRef]
130. Zhang, H.; Marma, M.S.; Bahl, S.K.; Kim, E.S.; McKenna, C.E. Sequence specific label-free DNA sensing using film-bulk-acoustic-resonators. *IEEE Sens. J.* **2007**, *7*, 1587–1588. [CrossRef]
131. Zheng, D.; Guo, P.; Xiong, J.; Wang, S. Streptavidin modified ZnO film bulk acoustic resonator for detection of tumor marker mucin 1. *Nanoscale Res. Lett.* **2016**, *11*, 1–8. [CrossRef]
132. Lin, A.; Li, Y.-J.; Wang, L.; Chen, S.-J.; Gross, M.E.; Kim, E.S. Label-free detection of prostate-specific antigen with FBAR-based sensor with oriented antibody immobilization. In *2011 IEEE International Ultrasonics Symposium*; IEEE: Piscataway, NJ, USA, 2011.
133. Zhao, X.; Pan, F.; Ashley, G.M.; Garcia-Gancedo, L.; Luo, J.; Flewitt, A.J.; Milne, W.I.; Lu, J.R. Label-free detection of human prostate-specific antigen (hPSA) using film bulk acoustic resonators (FBARs). *Sens. Actuators B Chem.* **2014**, *190*, 946–953. [CrossRef]
134. Chen, D.; Wang, J.; Li, D.; Li, Z. Film bulk acoustic resonator based biosensor for detection of cancer serological marker. *Electron. Lett.* **2011**, *47*, 1169–1170. [CrossRef]
135. Markets, R.A. Acoustic Wave Sensor Market-Forecasts from 2021 to 2026. 2021. Available online: [https://www.researchandmarkets.com/reports/5510697/acoustic-wave-sensor-market-forecasts-from-2021?gclid=EAIaIQobChMI3ZGzr8SR\\_AIVU1pgCh2WYwDkEAAYASAAEgLyd\\_D\\_BwE](https://www.researchandmarkets.com/reports/5510697/acoustic-wave-sensor-market-forecasts-from-2021?gclid=EAIaIQobChMI3ZGzr8SR_AIVU1pgCh2WYwDkEAAYASAAEgLyd_D_BwE) (accessed on 8 December 2022).
136. Girvin, S.M.; Yang, K. *Modern Condensed Matter Physics*; Cambridge University Press: Cambridge, UK, 2019.
137. Gustafsson, M.V.; Santos, P.V.; Johansson, G.; Delsing, P. Local probing of propagating acoustic waves in a gigahertz echo chamber. *Nat. Phys.* **2012**, *8*, 338–343. [CrossRef]
138. Takada, S.; Edlbauer, H.; Lepage, H.V.; Wang, J.; Mortemousque, P.-A.; Georgiou, G.; Barnes, C.H.; Ford, C.J.; Yuan, M.; Santos, P.V. Sound-driven single-electron transfer in a circuit of coupled quantum rails. *Nat. Commun.* **2019**, *10*, 1–9. [CrossRef]
139. Delsing, P.; Cleland, A.N.; Schuetz, M.J.; Knörzer, J.; Giedke, G.; Cirac, J.I.; Srinivasan, K.; Wu, M.; Balram, K.C.; Bäuerle, C. The 2019 surface acoustic waves roadmap. *J. Phys. D Appl. Phys.* **2019**, *52*, 353001. [CrossRef]
140. Averin, D.; Likharev, K. Coulomb blockade of single-electron tunneling, and coherent oscillations in small tunnel junctions. *J. Low Temp. Phys.* **1986**, *62*, 345–373. [CrossRef]
141. Hsiao, T.-K.; Rubino, A.; Chung, Y.; Son, S.-K.; Hou, H.; Pedrós, J.; Nasir, A.; Éthier-Majcher, G.; Stanley, M.J.; Phillips, R.T. Single-photon emission from single-electron transport in a SAW-driven lateral light-emitting diode. *Nat. Commun.* **2020**, *11*, 1–7. [CrossRef] [PubMed]
142. Zhang, X.; Zou, C.; Jiang, L.; Tang, H.X. Superstrong coupling of thin film magnetostatic waves with microwave cavity. *J. Appl. Phys.* **2016**, *119*, 023905. [CrossRef]
143. Tabuchi, Y.; Ishino, S.; Ishikawa, T.; Yamazaki, R.; Usami, K.; Nakamura, Y. Hybridizing ferromagnetic magnons and microwave photons in the quantum limit. *Phys. Rev. Lett.* **2014**, *113*, 083603. [CrossRef] [PubMed]
144. Bhoi, B.; Cliff, T.; Maksymov, I.; Kostylev, M.; Aiyar, R.; Venkataramani, N.; Prasad, S.; Stamps, R. Study of photon–magnon coupling in a YIG-film split-ring resonant system. *J. Appl. Phys.* **2014**, *116*, 243906. [CrossRef]
145. Noguchi, A.; Yamazaki, R.; Tabuchi, Y.; Nakamura, Y. Qubit-assisted transduction for a detection of surface acoustic waves near the quantum limit. *Phys. Rev. Lett.* **2017**, *119*, 180505. [CrossRef]

146. An, K.; Litvinenko, A.N.; Kohno, R.; Fuad, A.A.; Naletov, V.V.; Vila, L.; Ebels, U.; de Loubens, G.; Hurdequint, H.; Beaulieu, N. Coherent long-range transfer of angular momentum between magnon Kittel modes by phonons. *Phys. Rev. B* **2020**, *101*, 060407. [[CrossRef](#)]
147. Hayashi, H.; Ando, K. Spin pumping driven by magnon polarons. *Phys. Rev. Lett.* **2018**, *121*, 237202. [[CrossRef](#)]
148. Weiler, M.; Dreher, L.; Heeg, C.; Huebl, H.; Gross, R.; Brandt, M.S.; Gönnerwein, S.T. Elastically driven ferromagnetic resonance in nickel thin films. *Phys. Rev. Lett.* **2011**, *106*, 117601. [[CrossRef](#)]
149. Zhao, C.; Zhang, Z.; Li, Y.; Zhang, W.; Pearson, J.E.; Divan, R.; Liu, Q.; Novosad, V.; Wang, J.; Hoffmann, A. Direct imaging of resonant phonon-magnon coupling. *Phys. Rev. Appl.* **2021**, *15*, 014052. [[CrossRef](#)]
150. Casals, B.; Statuto, N.; Foerster, M.; Hernández-Mínguez, A.; Cicheler, R.; Manshausen, P.; Mandziak, A.; Aballe, L.; Hernández, J.M.; Macià, F. Generation and imaging of magnetoacoustic waves over millimeter distances. *Phys. Rev. Lett.* **2020**, *124*, 137202. [[CrossRef](#)] [[PubMed](#)]
151. Streib, S.; Keshtgar, H.; Bauer, G.E. Damping of magnetization dynamics by phonon pumping. *Phys. Rev. Lett.* **2018**, *121*, 027202. [[CrossRef](#)] [[PubMed](#)]
152. Berk, C.; Jaris, M.; Yang, W.; Dhuey, S.; Cabrini, S.; Schmidt, H. Strongly coupled magnon-phonon dynamics in a single nanomagnet. *Nat. Commun.* **2019**, *10*, 1–6. [[CrossRef](#)] [[PubMed](#)]
153. Yahiro, R.; Kikkawa, T.; Ramos, R.; Oyanagi, K.; Hioki, T.; Daimon, S.; Saitoh, E. Magnon polarons in the spin Peltier effect. *Phys. Rev. B* **2020**, *101*, 024407. [[CrossRef](#)]
154. Godejohann, F.; Scherbakov, A.V.; Kukhtaruk, S.M.; Poddubny, A.N.; Yaremkevich, D.D.; Wang, M.; Nadzeyka, A.; Yakovlev, D.R.; Rushforth, A.W.; Akimov, A.V. Magnon polaron formed by selectively coupled coherent magnon and phonon modes of a surface patterned ferromagnet. *Phys. Rev. B* **2020**, *102*, 144438. [[CrossRef](#)]
155. Yin, T.-S.; Jin, G.-R.; Chen, A. Enhanced Phonon Antibunching in a Circuit Quantum Acoustodynamical System Containing Two Surface Acoustic Wave Resonators. *Micromachines* **2022**, *13*, 591. [[CrossRef](#)] [[PubMed](#)]
156. Kuzyk, M.C.; Wang, H. Scaling phononic quantum networks of solid-state spins with closed mechanical subsystems. *Phys. Rev. X* **2018**, *8*, 041027. [[CrossRef](#)]
157. Schütz, M.J. Universal quantum transducers based on surface acoustic waves. In *Quantum Dots for Quantum Information Processing: Controlling and Exploiting the Quantum Dot Environment*; Springer: Cham, Switzerland, 2017; pp. 143–196.
158. Buller, J.; Balderas-Navarro, R.; Biermann, K.; Cerda-Méndez, E.; Santos, P. Exciton-polariton gap soliton dynamics in moving acoustic square lattices. *Phys. Rev. B* **2016**, *94*, 125432. [[CrossRef](#)]
159. Couto, O.; Lazić, S.; Iikawa, F.; Stotz, J.; Jahn, U.; Hey, R.; Santos, P. Photon anti-bunching in acoustically pumped quantum dots. *Nat. Photonics* **2009**, *3*, 645–648. [[CrossRef](#)]
160. Metcalfe, M.; Carr, S.M.; Muller, A.; Solomon, G.S.; Lawall, J. Resolved sideband emission of InAs/GaAs quantum dots strained by surface acoustic waves. *Phys. Rev. Lett.* **2010**, *105*, 037401. [[CrossRef](#)]
161. Blattmann, R.; Krenner, H.J.; Kohler, S.; Hänggi, P. Entanglement creation in a quantum-dot-nanocavity system by Fourier-synthesized acoustic pulses. *Phys. Rev. A* **2014**, *89*, 012327. [[CrossRef](#)]
162. Pustiowski, J.; Müller, K.; Bichler, M.; Koblmüller, G.; Finley, J.J.; Wixforth, A.; Krenner, H.J. Independent dynamic acousto-mechanical and electrostatic control of individual quantum dots in a LiNbO<sub>3</sub>-GaAs hybrid. *Appl. Phys. Lett.* **2015**, *106*, 013107. [[CrossRef](#)]

**Disclaimer/Publisher’s Note:** The statements, opinions and data contained in all publications are solely those of the individual author(s) and contributor(s) and not of MDPI and/or the editor(s). MDPI and/or the editor(s) disclaim responsibility for any injury to people or property resulting from any ideas, methods, instructions or products referred to in the content.